Louisiana Tech University

Louisiana Tech Digital Commons

Summer 8-1-2022

LAYERED METAMATERIAL BEAM STRUCTURE WITH LOCAL RESONATORS FOR VIBRATION ATTENUATION: MODEL AND EXPERIMENT

Winner Chukwuzulum Anigbogu
Louisiana Tech University

LAYERED METAMATERIAL BEAM STRUCTURE WITH LOCAL

RESONATORS FOR VIBRATION ATTENUATION: MODEL AND

EXPERIMENT

by

Winner Anigbogu, PhD. Candidate

A Dissertation Presented in Partial Fulfillment
of the Requirements of the Degree
Doctor of Philosophy

COLLEGE OF ENGINEERING AND SCIENCE
LOUISIANA TECH UNIVERSITY

August 2022

LOUISIANA TECH UNIVERSITY

GRADUATE SCHOOL

July 7, 2022

Date of dissertation defense

We hereby recommend that the dissertation prepared by
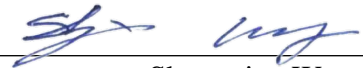
Winner Chukwuzulum Anigbogu, M. S.

entitled   **LAYERED METAMATERIAL BEAM STRUCTURE WITH**

LOCAL RESONATORS FOR VIBRATION ATTENUATION: MODEL AND

 EXPERIMENT

be accepted in partial fulfillment of the requirements for the degree of

Doctor of Philosophy in Engineering, Micro & Nanoscale Systems Conc.

Hamzeh Bardaweel
Supervisor of Dissertation Research

Shengnian Wang
Head of Engineering

Doctoral Committee Members:
Sandra Zivanovic
Leland Weiss
Arden Moore
Arun Jaganathan

Approved:

Hisham Hegab
Dean of Engineering & Science

Approved:

Ramu Ramachandran
Dean of the Graduate School

ABSTRACT

Layered metamaterial beam structures are gaining attention in a variety of fields including vibration attenuation and energy harvesting. Exhaustive research on single-beam metamaterial vibration attenuation structures using local resonators exists in literature. Moreover, there are recent attempts at modelling double-layered beams with different kinds of constraints. The double-layered beam models in literature are limited to simple beams and not extended to metamaterials with local resonators. This research is primarily focused on developing a design criterion and a modelling platform for layered metamaterial structures with multiple beams and local resonators for vibration isolation. The model is developed using Euler-Bernoulli beam equations, superposition of mode shapes and Galerkin methods. A prototype layered metamaterial structure is fabricated and characterized experimentally. The prototype consists of horizontal beams, local resonators forming unit cells, and vertical beams linkages. Each local resonator consists of cantilevers with tip masses. Results show good agreement between model and experiment. Two major bandgaps are observed at 190 Hz – 410 Hz and 550 Hz – 710 Hz. Results reveal that the low frequency bandgap can be further reduced through the design of the local resonators. Results also show that alternating the length of the local resonators causes a shift in the first frequency bandgap. An increase in the number of local resonators opens up extra frequency bandgaps at lower frequencies with the drawback of reducing the depth in vibration transmissibility. Moreover, the higher

frequency bandgaps are mostly affected by the horizontal beams. An increase in the length of the horizontal beams, while the number and design of the local resonators are fixed, broadens the second frequency bandgap and shifts it to lower frequency values. Additionally, the ability of the fabricated metamaterial structure to harvest electric power in these bandgaps is examined. Results show that vibration attenuation and energy harvesting characteristics of the metamaterial structure are coupled. Stronger vibration attenuation within the first bandgap has led to enhanced energy harvesting capabilities within this bandgap. Power measurements at optimum load resistance of 15 Ω reveal that maximum power generated within the first bandgap reaches 5.2 μW at 245 Hz. Compared to state-of-the-art, the metamaterial structure presented here shows a significant improvement in electric power generation, at considerably lower load resistance, while maintaining the ability to attenuate undesired vibrations within the frequency bandgap. Lastly, the comparative advantages of layered-beam structures over single-beam metamaterial structures is studied. A beam prototype and dimension studied by multiple articles in literature is used in simulating the comparative study. Results show that in cases where spacing and design of the local resonators are desired to remain fixed, layering the horizontal beams offers a significant pathway for both lowering the bandgap and developing additional bandgaps. Results also suggest that increasing the number of resonators per horizontal beam further generates multiple lower bandgaps in layered metamaterial beams. In situations where the number of local resonators per beam are desired to remain constant, increasing the length of the unit-cells offers an alternative technique for lowering the bandgaps. This comparative study is particularly useful to engineers and researchers designing applications of beam-type metamaterial structures.

APPROVAL FOR SCHOLARLY DISSEMINATION

The author grants to the Prescott Memorial Library of Louisiana Tech University the right to reproduce, by appropriate methods, upon request, any or all portions of this Dissertation. It is understood that "proper request" consists of the agreement, on the part of the requesting party, that said reproduction is for his personal use and that subsequent reproduction will not occur without written approval of the author of this Dissertation. Further, any portions of the Dissertation used in books, papers, and other works must be appropriately referenced to this Dissertation.

Finally, the author of this Dissertation reserves the right to publish freely, in the literature, at any time, any or all portions of this Dissertation.

Author _____

Date _____

DEDICATION

      This dissertation is dedicated to my wife who was a consistent source of encouragement throughout my time in graduate school. This work is also dedicated to my parents for their immense support through their words and prayers. My family stood by me through the ups and downs of my doctorate journey, and I am deeply grateful to have them in my life.

TABLE OF CONTENTS

LIST OF FIGURES

LIST OF TABLES

ACKNOWLEDGMENTS

CHAPTER 1

INTRODUCTION

1.1   Motivation

Recently, mechanical metamaterials have become the focus of many research studies and engineering applications [1]. This increase in attention stems from their unique properties including the presence of frequency bandgaps influenced by the local resonators [2], [3]. Metamaterials have found use-cases particularly in many engineering applications including wave guiding, vibration attenuation and, more recently, dual-purpose vibration suppression and energy scavenging [4]–[6]. Frequency bandgaps developed in these metamaterial structures originate from the ability of the local resonators to trap kinetic energy from the oscillations passing through the metamaterial structure. Single-beam metamaterial structures have been studied exhaustively as vibration isolation systems [7]–[12]. The literature reveals that a growing number of researchers have recently attempted to use layered-beam metamaterial structures for simultaneous vibration attenuation and energy harvesting. The work in this area is still new and rapidly evolving [13]. It is therefore important to develop a generic modeling platform for layered metamaterial structures with multiple beams and multiple local resonators per beam. The desire to develop a generic platform for layered metamaterial beam structure modelling informed the commencement of this research work. The availability of a generic modelling platform for metamaterials will be vital for engineers

seeking to simply focus on designing application use-cases of layered beam metamaterial structures. Additionally, the ability of such layered-beam metamaterial systems to simultaneously generate power while isolating vibrations is also verified. Studying the power generation capacity of the system was motivated by a recent work by researchers in Duke University that showed a metamaterial structure that harnessed power at the efficiency of solar cells [7].

1.2   Objectives

The primary focus of this research work is on developing a generic platform for modelling layered metamaterial structures with multiple horizontal beam and local resonators. The model is developed in a manner that could be replicated in modelling varying number of horizontal-beams of a layered metamaterial structure with varying number of local resonators per horizontal-beam. The semi-analytical model is developed using Euler-Bernoulli beam equations, superposition of mode shapes and Galerkin methods. Runge-Kutta method is used to solve the equations developed from the semi-analytical model.

To ascertain the accuracy of the semi-analytical model developed, COMSOL FEM software is used to analyze the dispersion curve of the layered-beam metamaterial structure and displacement of the resonators. In COMSOL analysis, the layered metamaterial structure is broken into its unit-cell and Bloch-Floquet's periodic boundary condition is applied to the boundaries. The resonant frequency of the local resonators is deduced in COMSOL and compared with the result from the semi-analytical model. Also, the displacement of the unit cell at frequencies within the bandgaps predicted by

the semi-analytical model is studied. The dispersion curve from COMSOL analysis is used to reveal the predictable bandgap zone of the layered-beam metamaterial structure.

Furthermore, Eigen-Value equation is developed using the continuity equation of the horizontal beams of the layered-beam metamaterial structure. The equation is used to develop a second dispersion curve for analyzing and predicting the frequency bandgap regions of the layered-beam metamaterial structure. This bandgap from the Eigen-frequency equation is compared with the bandgap seen in the COMSOL model and used to validate the semi-analytical model. For application purposes, the ability of the layered-beam metamaterial structure to convert trapped mechanical vibration energy into electric power is investigated. A magneto-motive transducer is used in energy conversion. Lastly, a comparative analysis of bandgap generating capacity of single-beam metamaterial structure and layered-beam metamaterial structure of the same sort is modeled. The comparative study is important to cater for the knowledge-base of engineers and researchers with interest in developing application use-cases of beam-type metamaterial beam structures.

CHAPTER 2

LITERATURE REVIEW

In this chapter, the progression of various works presented by researchers in the literature from the basic concept of metamaterials to the stage where this work adds value to literature is presented. Firstly, the efforts of researchers in understanding the working-principles of metamaterials are elaborated. Next, various research efforts on single-beam metamaterial structure reported in the literature are presented. It is promptly followed by evaluation of different efforts by researchers to evolve beam-type metamaterial structures from single-beam metamaterial structure to layered-beam metamaterial structure. The application use-cases of these beam-type metamaterial structures reported in the literature are also outlined, particularly their use as dual-purpose vibration isolation energy harvesting devices. Lastly, the research gaps that necessitated this work are outlined, giving credence to the vital value this works adds to the body of literature in mechanical metamaterials. Some parts of this chapter come from two previously published journal articles: **1.** Winner Anigbogu, Hamzeh Bardaweel, "A Metamaterial-Inspired Structure for Simultaneous Vibration Attenuation and Energy Harvesting", Shock and Vibration, vol. 2020, Article ID 4063025, 12 pages, 2020. https://doi.org/10.1155/2020/4063025 and **2.** Anigbogu, Winner., Nguyen, Hieu., and Bardaweel, Hamzeh. "Layered Metamaterial Beam Structures With Local Resonators for Vibration Attenuation: Model and Experiment." Frontiers in Mechanical Engineering Vol. 7 (2021).

4

https://doi.org/10.3389/fmech.2021.768508. Permission was obtained from all the co-authors involved in the published studies.

2.1   Metamaterial Principle

Local-resonator frequency bandgaps in metamaterial structures originate from the ability of the local resonators to absorb kinetic energy from the oscillations passing through the metamaterial structure [14]. When the frequency of the external vibration source aligns with the resonant frequency of the local resonators, energy from these oscillations is transferred to the local resonators [14], [15]. Typically, these local resonators are either attached to the surface of the metamaterial structures or embedded inside [15]–[17]. Additionally, the Bragg's scattering in the periodic structures leads to generation of frequency bandgaps [18]. The bandgaps generated by Bragg's scattering are influenced by the wavelengths of the Bragg scattering mechanism, which is limited by the design of the beam of the mechanical metamaterial structure [15]. The addition of local resonators to the structure makes it possible to generate bandgaps at frequencies much lower than the Bragg's frequencies [19], [20]. In the case of vibration attenuation, when the mechanical metamaterial is subject to vibrations by an external vibration source, it has the ability to suppress these oscillations, at low frequencies, that are closely aligned with the resonant frequency of the local resonators [21].

2.2   Single-Beam Metamaterial Structures

Exhaustive literature has already looked at design criteria and characterization of metamaterial structures that are made of single beam structures with local resonators [10]–[12], [22]–[24]. For example, the work by Liu et al. was among the first few studies to look at metamaterial structures and local resonators [19]. Their pioneer seminal work showed

that localized resonant structures exhibit valuable characteristics such as negative elastic constants, leading to generation of low frequency bandgaps. The transfer matrix method was then used by Yu et al. for characterization of a single beam metamaterial structure with resonators that are made of rubber and copper rings [10], [11]. The results from their model simulations were validated experimentally. Xiao et al. built on the analytical model of the single beam metamaterial design developed by Yu et al. and showed that resonance and Bragg's bandgaps exist as a result of local resonance effect and periodicity of unit cells [22]. Liu et al. further studied the effects of different design parameters on the generated frequency bandgaps [25]. The results from their work revealed that, although a large local resonator generates wide attenuation, a large number of small local resonators spread across the beam gives enhanced attenuation spectra.

Other enhanced designs and studies of single beam-based metamaterial structures have also been developed [23], [24], [26]–[28]. For instance, a design of a beam with spring-mass local resonators sandwiched inside the beam was proposed by Chen et al. [26]. Their results showed that the amplitude of waves was attenuated near the resonance frequency of the local resonators. Additionally, their results revealed that bandgaps were influenced mostly by the size of the internal mass rather than the spring constant of the resonator. To create more flexible bandgaps, Xiao et al. designed an array of local resonators with varying resonant frequencies [27]. Their work showed that, compared to a beam with a single array of local resonators, a beam with varying array of local resonators can generate broader bandgaps above and below Bragg's bandgap. Zhou et al. used a combination of both vertical springs and oblique springs to investigate the effect of negative stiffness introduced by the oblique springs on single beam-based

metamaterial structures [12]. Their results showed that adding two oblique springs to the single beam-based metamaterial structure introduced negative stiffness which effectively produced attenuation at lower frequencies. More recently, Xia et al. studied the effect of nonlinearity that was purposefully introduced into the design of a single beam-based metamaterial structure [1]. This was done by adding bi-stable attachments to the metamaterial structure. Their work showed that nonlinear vibrations of the bi-stable resonator attachments resulted in wider frequency bandgap compared to the case when only linear local resonators were considered.

2.2.1   Layered-Beam Metamaterial Structure

While on the one hand all the aforementioned studies have focused on single-beam based metamaterial structures with local resonators. On the other hand, few recent studies have looked at modelling layered beams. For example, Oniszczuk investigated two beams connected by a Winker elastic layer [29]. The work used Bernoulli-Fourier method to show that the free vibration of a simply supported double-beam system is similar to a double-string system. Li et al. used both Fourier and Laplace approach to develop a closed form solution for double infinite Euler-Bernoulli beams with harmonic loads applied [30]. Douglas et al. treated a system of three elastic-viscoelastic beams as two non-identical Euler-Bernoulli beams with a viscoelastic layer between them [31]. The method was limited to a specific fixed-free boundary condition and an external load applied only at the free end. Vu et al. extended Euler-Bernoulli's approach to arbitrary boundary conditions and applied loads [32]. Abu-Hilal then applied a change of variable method in decoupling the set of fourth-order differential equations from the modal solution of double Euler-Bernoulli beams with moving loads [33]. Li et al. recently demonstrated the use of layered

metamaterial for simultaneous vibration isolation and energy harvesting [14]. Anigbogu et al. presented a unique metamaterial design using 3D printed layered beams to achieve vibration attenuation [34]. Their results showed that layered metamaterial beams can achieve vibration attenuation at low frequencies that are commonly encountered in nature. A key observation from these recent studies is that these efforts have mainly focused on studying and investigating either single beam-based metamaterial structures or double-beams with different support systems. None of these studies has tackled the issue of developing a general approach to modelling layered metamaterial beams with local resonators. Recently, these layered metamaterial beams with local resonators have found numerous potential engineering applications including vibration attenuation and energy scavenging [14], [34].

2.3   Dual-Purpose Vibration Isolation Energy Harvesters

A thorough review of metamaterials-based energy harvesters was presented by Chen et al. [35]. For example, a metamaterial energy harvester employing piezoelectrics was fabricated [36]. The harvester was shown to produce peak power in the order of 100 μW-1 mW at 55 kHz and 30-80 kΩ. Concurrent vibration attenuation and energy harvesting metamaterials have also been demonstrated recently. Chen et al. built a metamaterial beam embedded with periodic cells that consist of membrane-split-ring resonators [37]. PVDF piezoelectric patch was attached to the membranes to convert the kinetic energy captured by the resonators into useful electric power. The fabricated structure exhibited simultaneous vibration attenuation and energy harvesting capabilities. Excellent and moderate vibration attenuation characteristics were reported in two bandgaps, i.e. 340-426 Hz and 460-500 Hz, respectively. The fabricated structure

recovered approximately 0.5 µW across 200 kΩ at 348 Hz. Power was only measured and reported within the first bandgap, i.e. at 348 Hz. Also, a recent study by Li et al. reported a mechanical metamaterial structure for simultaneous vibration isolation and energy harvesting [14]. The structure consisted of beams with PVDF piezoelectric transducers to extract electric energy from the resonating cells. The metamaterial structure was able to attenuate vibrations and generate electric power, simultaneously, within 146-171 Hz frequency bandgap. Specifically, a peak power of 0.05 µW was measured across 1 MΩ within the frequency bandgap. The current state-of-the-art literature reveals that a growing number of researchers have recently attempted to use elastic mechanical metamaterials for simultaneous vibration attenuation and energy harvesting.

The work presented in this article is motivated by the growing interest in layered metamaterial beams with local resonators. To the best knowledge of the authors, the work presented here is the first to tackle the issue of developing a modelling platform for layered metamaterial structures with multiple beams and local resonators. The work is focused on developing design criteria and modelling platform for layered metamaterial structures with multiple beams and local resonators. The model is developed using Galerkin method and superposition of mode shapes to solve an application of Euler-Bernoulli equation to layered-metamaterial beam structures. A prototype of the layered metamaterial structure with local resonators is fabricated and characterized experimentally. The model developed in this work is then validated against measured data.

Research interest in the use of layered-beam metamaterial structure for energy harvesting is growing [13]. Therefore, the work we present in this article additionally investigates the structures ability to serve as a magneto-mechanical based metamaterial structure for simultaneous vibration attenuation and energy harvesting. A permanent magnet-coil systems is added to the layered-beam metamaterial structure in order to achieve two main functions, simultaneously. These functions are vibration attenuation and energy harvesting. Compared to other efforts and available literature, the metamaterial structure we present in this work is shown to generate, significantly, more electric power while maintaining its ability to attenuate undesired vibrations. Additionally, the presented structure requires lower load resistance to achieve optimum power transfer, compared to what has been presented in the literature[14], [36], [37]. This is an important feature of the presented structure because, typically, electronic circuits for sensors require an input current in the order of 10 mA [38]. As the load resistance increases the deliverable electric current decreases. Therefore, it is desirable to achieve maximum power transfer at the lowest load resistance values [38].

Since layered metamaterial beam structures with local resonators are finding a growing engineering potential, it is important to additionally study the advantages in bandgap generation offered by these layered metamaterial structures over typical single beam metamaterial structures. In the application of metamaterial beam structures as dual-purpose systems for electric power generation, the more the local resonators (unit-cells) per miniature device, the more the aggregate electric power generation potential of the device. This is because the electromechanical transducers are usually placed on the local resonators. In such cases, having a layered metamaterial structure is physically an

attractive choice. Also, because the existence of multiple bandgaps is very desirable in such structures, a comparative analysis and design study between layered and single beam metamaterial structures is important. An awareness of these advantages can help researchers in designing metamaterial beam structures for various applications including vibration attenuation and energy harvesting. A standard single beam metamaterial structure is analyzed, its transmissibility bandgap and enhancements are presented. Afterwards, a simple double-layered metamaterial beam structure is modelled and the bandgaps of the layered metamaterial structures are presented and compared with single beam metamaterial structure. Lastly, parametric and design studies that investigate the effects of changes in various parameters of the double-layered metamaterial beam structure are presented and the outcomes are compared with the results from single beam metamaterial structures.

CHAPTER 3

DESIGN AND MODEL DEVELOPMENT

This chapter focuses on introducing the design approach used in developing the generic modelling platform for layered-beam metamaterial structures proposed in this work. The details of the semi-analytical model used in analyzing the transmissibility of the layered-beam metamaterial structures are also outlined in this chapter. Additionally, COMSOL finite element model and Eigen-value model equations for the layered-beam metamaterial structure are presented in this chapter. This chapter has contents adopted from two previously published journal articles: **1.** Winner Anigbogu, Hamzeh Bardaweel, "A Metamaterial-Inspired Structure for Simultaneous Vibration Attenuation and Energy Harvesting", Shock and Vibration, vol. 2020, Article ID 4063025, 12 pages, 2020. https://doi.org/10.1155/2020/4063025 and **2.** Anigbogu, Winner., Nguyen, Hieu., and Bardaweel, Hamzeh. "Layered Metamaterial Beam Structures With Local Resonators for Vibration Attenuation: Model and Experiment." Frontiers in Mechanical Engineering Vol. 7 (2021). https://doi.org/10.3389/fmech.2021.768508.Permission was obtained from all the co-authors involved in the published studies.

3.1   Design

The overall representation of the layered metamaterial vibration attenuation structure is shown in **Figure 3-1a**. The metamaterial structure is comprised of J-layered horizontal beams, the local resonators per unit cell and the vertical beams linking the

horizontal beams together. The local resonators are made of cantilevers with tip masses attached to them as shown in **Figure 3-1a**. Each unit cell has four local resonators linked to the same point as shown in **Figure 3-1b**. For simplicity we represent the unit cell as one single local resonator force acting on the same point, in tandem with the approach adopted by Wang et al. [23]. The effects of the vertical beams are factored into the governing equations as spring forces and damping forces following the relative velocities of the beams as shown in **Figure 3-2**. The free body diagram of the local resonators within a unit cell is shown in **Figure 3-3**. An approximate model of the transmissibility of the layered metamaterial structure is obtained using Euler-Bernoulli's equations and Galerkin method [12].
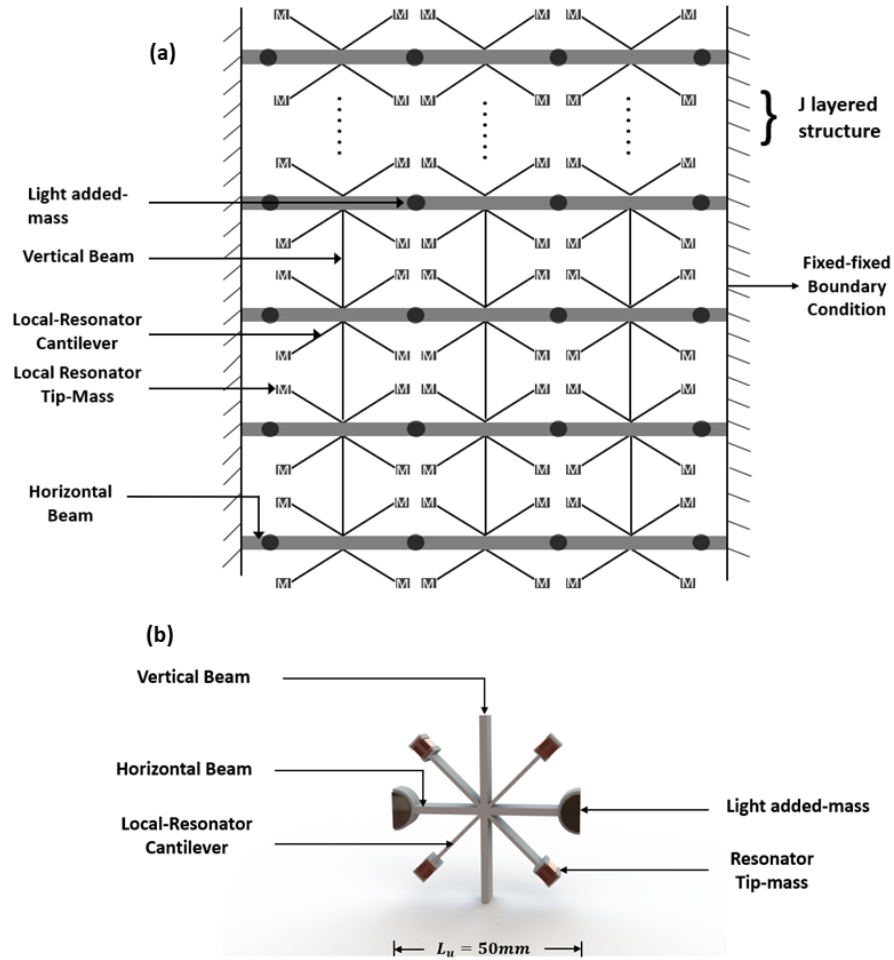
Figure 3-1: Schematic description of a j-layered metamaterial structure and its coupled parts: **(a)** Layered metamaterial structure constituents including horizontal beams, vertical beams and local resonators, and **(b)** Representation of the basic unit cell of the layered metamaterial assembly. It is comprised of local resonators with tip masses and vertical columns attached to the beam. The length of a unit cell is 50mm
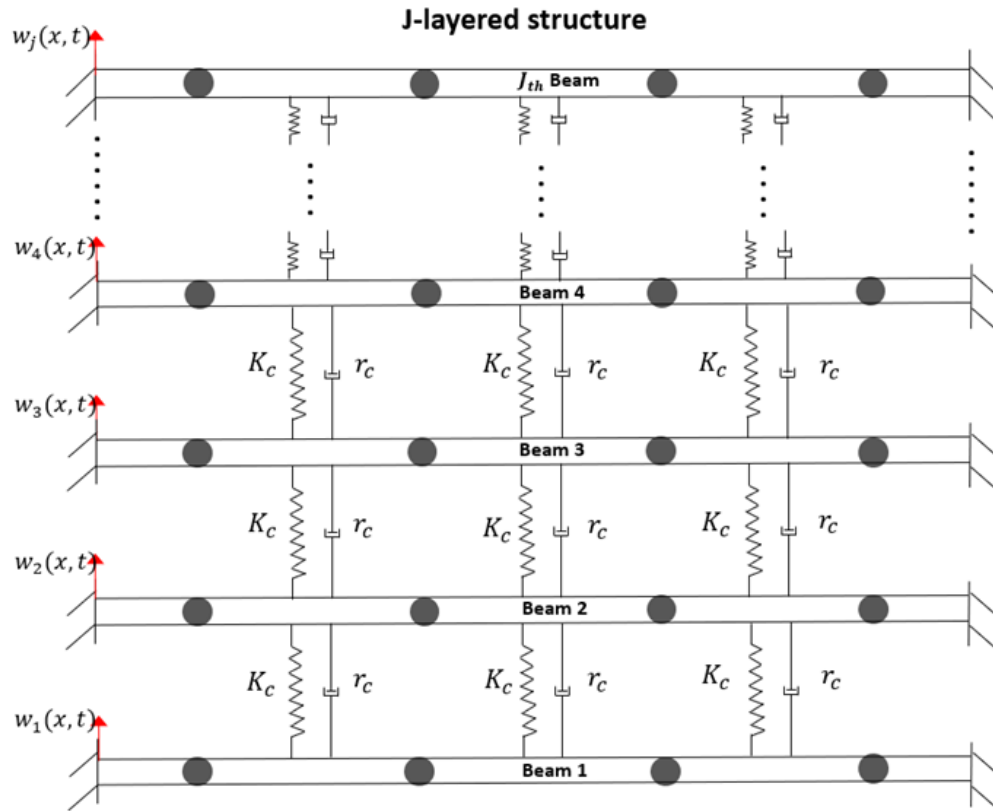
Figure 3-2: Schematic diagram of the free body diagram for the vertical beams attached to each unit cell and between the horizontal beams of a j-layered metamaterial structure.
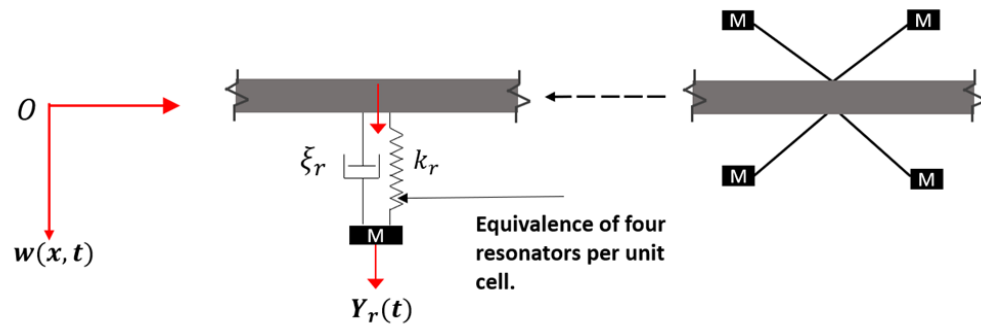
Figure 3-3: Free body diagram of a local resonator. The four local resonators acting at a point in the unit cell are reduced into an equivalent single local resonator unit cell in the model.

3.2   Semi-Analytical Model

3.2.1   Layered-Beam Model Development

In order to analyze the dynamic behavior of the layered metamaterial vibration attenuation structure when subject to external vibrations, the Frequency Response Function (FRF) approach is used to determine the transmissibility of the device. The Galerkin method is applied in analyzing the layered-beam metamaterial structures' response to external vibrations. The length of each horizontal beam is given as $L = \alpha * L_u$, where α is the number of unit cells, and L_u is the length of each unit cell in the design adopted in this work (**Figure 3-1b**). The transverse vibration of a simple beam with attachment and a vibration source at a point is given by the standard Euler Bernoulli equation [12]:

$$EI\frac{\partial^4 w_i}{\partial x^4} + \rho A\frac{\partial^2 w_i}{\partial t^2} = f_s(x,t)\delta\left(x - \frac{L}{2}\right) + \sum_{r=1}^{n} f(x_r,t)\delta(x - x_r) \qquad \textbf{Eq. 3-1}$$

where w, E and I are the transverse displacement, Young's modulus of elasticity and the cross-sectional moment of inertia of the beam, respectively. Moreover, ρ and A are the density of the material, and the cross-sectional area of the beam, respectively. The expressions f_s, δ and f represent the force from the vibration source, the delta Dirac function and the force from the attached local resonators, respectively. The force, f_s, from the vibration source only applies to the first beam. In **Eq. 3-1**, x_r represents the position of the local resonator, while n is the total number of local resonators on each horizontal beam. This Euler Bernoulli equation shown in **Eq. 3-1** is used to analyze the displacement of each of the i_{th} horizontal beams. Applying Galerkin method and the

superposition of modes, the transverse displacement of i_{th} horizontal beam, w_i is given by [12]:

$$w(x,t)_{i=1,2,\dots,j} = \sum_{q=1}^{N} u_{iq}(t)\emptyset_{iq}(x) \qquad \textbf{Eq. 3-2}$$

In **Eq. 3-2**, u_{iq} is the generalized displacement of the i_{th} horizontal beam at the q_{th} mode, and $\emptyset_{iq}$ is the trial function of the i_{th} horizontal beam which is taken to be the mode shape of the horizontal beam at the q_{th} mode. The index j is the total number of layered horizontal beams.

Next, we extend **Eq. 3-1** to factor in the connecting vertical beams as shown in **Figure 3-1** and **Figure 3-2**. This yields the set of equations representing each of the horizontal beams from the base-beam to the top, respectively. A generalized form of this set of equations from the lowest horizontal beam, i.e., $i = 1$, to i_{th} middle horizontal beam, i.e., $i = 2:j - 1$, till the j_{th} topmost beam, i.e., $i = j$, for any j number of horizontal beams constituting the layered metamaterial structure yields **Eq. 3-3** - **Eq. 3-7** below [29]:

$$\begin{cases} EI\frac{\partial^4 w_i}{\partial x^4} + k_c(w_i - w_{i+1}) + r_c(\dot{w}_i - \dot{w}_{i+1}) + \rho A\frac{\partial^2 w_i}{\partial t^2} = f_s(x,t)\delta\left(x - \frac{L}{2}\right) + \sum_{r=1}^{n} f(x_r,t)\delta(x - x_r), & i = 1 \\ EI\frac{\partial^4 w_i}{\partial x^4} + k_c(w_i - w_{i-1}) + k_c(w_i - w_{i+1}) + r_c(\dot{w}_i - \dot{w}_{i-1}) + r_c(\dot{w}_i - \dot{w}_{i+1}) + \rho A\frac{\partial^2 w_i}{\partial t^2} = \sum_{r=1}^{n} f(x_r,t)\delta(x - x_r), & i = 2:j-1 \\ EI\frac{\partial^4 w_j}{\partial x^4} + k_c(w_j - w_{j-1}) + r_c(\dot{w}_j - \dot{w}_{j-1}) + \rho A\frac{\partial^2 w_j}{\partial t^2} = \sum_{r=1}^{n} f(x_r,t)\delta(x - x_r), & i = j \end{cases} \qquad \textbf{Eq. 3-3}$$

where $i = 1$ and $i = j$ are the lowest horizontal beam and topmost horizontal beam, respectively, and the middle section beams are indexed with $i = 2:j - 1$. In **Eq. 3-3**, f_s is the force exerted by the vibration source, represented as a sinusoidal input $f_s = F_A \cos \omega t$. Also ω is the forcing frequency of vibration source, F_A is the amplitude of

the external vibration force and k_c represents the stiffness of the vertical beams given by [39]:

$$k_c = \frac{32 * E * b_c * h_c^3}{l_c^3}$$ **Eq. 3-4**

where b_c, h_c and l_c represent the width, thickness and length of the vertical beams respectively. The damping of each vertical beam, r_c, and the equivalent mass, m_c, are given by [40]:

$$r_c = 2\xi_c\sqrt{m_c k_c}$$ **Eq. 3-5**

$$m_c = 0.33 * \rho * A * l_c$$ **Eq. 3-6**

Grouping the impact of the vertical beams as forces acting at specific points on the horizontal beams, **Eq. 3-3** can be rewritten in the following generalized forms:

$$\begin{cases} EI\frac{\partial^4 w_i}{\partial x^4} + \rho A\frac{\partial^2 w_i}{\partial t^2} = f_s(x,t)\delta\left(x - \frac{L}{2}\right) + \sum_{r=1}^{n} f(x_r,t)\delta(x - x_r) + \sum_{c=1}^{v} f_i(x_c,t)\delta(x - x_c), & i = 1 \\ EI\frac{\partial^4 w_i}{\partial x^4} + \rho A\frac{\partial^2 w_i}{\partial t^2} = \sum_{r=1}^{n} f(x_r,t)\delta(x - x_r) + \sum_{c=1}^{v} f_i(x_c,t)\delta(x - x_c), & i = 2{:}j - 1 \\ EI\frac{\partial^4 w_j}{\partial x^4} + \rho A\frac{\partial^2 w_j}{\partial t^2} = \sum_{r=1}^{n} f(x_r,t)\delta(x - x_r) + \sum_{c=1}^{v} f_j(x_c,t)\delta(x - x_c), & i = j \end{cases}$$ **Eq. 3-7**

where $f_i(x_c, t)$ and $f_j(x_c, t)$ are the forces due to the vertical beams acting on each i_{th} horizontal beam (from the lowest horizontal beam to $j - 1_{th}$ horizontal beam) and the j_{th} topmost horizontal beam, respectively, and x_c represents the point of contacts on each horizontal beam. Using **Eq. 3-2**, these forces, which are due to the interlinking vertical beams, can be further developed into the following generalized set of equations:

$$\begin{cases} f_i(x_c,t) = -[k_c(w_i - w_{i+1}) + r_c(\dot{w}_i - \dot{w}_{i+1})], & i = 1 \\ f_i(x_c,t) = -[k_c(w_i - w_{i-1}) + k_c(w_i - w_{i+1}) + r_c(\dot{w}_i - \dot{w}_{i-1}) + r_c(\dot{w}_i - \dot{w}_{i+1})], & i = 2{:}j - 1 \\ f_j(x_c,t) = -[k_c(w_j - w_{j-1}) + r_c(\dot{w}_j - \dot{w}_{j-1})], & i = j \end{cases}$$ **Eq. 3-8**

Also, the forces from the attached local resonators and the internal damping force are given as:

$$f(x_r, t) = k_r[Y_r(t) - w(x_r, t)] \qquad\qquad \textbf{Eq. 3-9}$$

$$f_d(x_r, t) = 2\xi_r\sqrt{m_r k_r}\,[\dot{Y}_r(t) - \dot{w}(x_r, t)] \qquad\qquad \textbf{Eq. 3-10}$$

where $f_d(x_r, t)$, ξ_r and m_r are the internal damping force, the damping ratio and the

mass of the r_{th} local resonator, respectively. $Y_r(t)$ is the vertical displacement of the r_{th}

local resonator.

Substituting **Eq. 3-2** into **Eq. 3-7** yields the following set of equations, respectively:

$$\begin{cases} EI\sum_{q=1}^{N} u_{iq}(t)\emptyset_{iq}^{(iv)}(x) + \rho A\sum_{q=1}^{N} \ddot{u}_{iq}(t)\emptyset_{iq}(x) = f_s(x,t)\delta\left(x-\dfrac{L}{2}\right) + \sum_{r=1}^{n} f(x_r,t)\delta(x-x_r) + \sum_{c=1}^{v} f_i(x_c,t)\delta(x-x_c)\,, & i=1 \\[2mm] EI\sum_{q=1}^{N} u_{iq}(t)\emptyset_{iq}^{(iv)}(x) + \rho A\sum_{q=1}^{N} \ddot{u}_{iq}(t)\emptyset_{iq}(x) = \sum_{r=1}^{n} f(x_r,t)\delta(x-x_r) + \sum_{c=1}^{v} f_i(x_c,t)\delta(x-x_c)\,, & i=2{:}j-1 \\[2mm] EI\sum_{q=1}^{N} u_{jq}(t)\emptyset_{jq}^{(iv)}(x) + \rho A\sum_{q=1}^{N} \ddot{u}_{jq}(t)\emptyset_{jq}(x) = \sum_{r=1}^{n} f(x_r,t)\delta(x-x_r) + \sum_{c=1}^{v} f_j(x_c,t)\delta(x-x_c)\,, & i=j \end{cases} \quad \textbf{Eq. 3-11}$$

Multiplying **Eq. 3-11** by the trial function $\emptyset_{iy}(x)$, integrating over the length of

each of the horizontal beams, i.e., from 0 to L and applying orthogonality of mode

shapes, yields the following transformation:

$$\begin{cases} M_{iq}\ddot{u}_{iq}(t) + C_{iq}\dot{u}_{iq} + K_{iq}u_{iq} = f_s(x,t)\emptyset_{iq}\left(\dfrac{L}{2}\right) + \sum_{r=1}^{n}\emptyset_{iq}(x_r)f(x_r,t) + \sum_{r=1}^{n}\emptyset_{iq}(x_r)f_d(x_r,t) + \sum_{c=1}^{v}\emptyset_{iq}(x_c)f_i(x_c,t)\,, & i=1 \\[2mm] M_{iq}\ddot{u}_{iq}(t) + C_{iq}\dot{u}_{iq} + K_{iq}u_{iq} = \sum_{r=1}^{n}\emptyset_{iq}(x_r)f(x_r,t) + \sum_{r=1}^{n}\emptyset_{iq}(x_r)f_d(x_r,t) + \sum_{c=1}^{v}\emptyset_{iq}(x_c)f_i(x_c,t)\,, & i=2{:}j-1 \\[2mm] M_{jq}\ddot{u}_{jq}(t) + C_{jq}\dot{u}_{jq} + K_{jq}u_{jq} = \sum_{r=1}^{n}\emptyset_{jq}(x_r)f(x_r,t) + \sum_{r=1}^{n}\emptyset_{jq}(x_r)f_d(x_r,t) + \sum_{c=1}^{v}\emptyset_{jq}(x_c)f_j(x_c,t)\,, & i=j \end{cases} \quad \textbf{Eq. 3-12}$$

Here, the transverse displacements, $w(x, t)_{i=1,2,\dots,j}$, in the forces $f(x_r, t)$,

$f_d(x_r, t)$ and $f_i(x_c, t)$ in **Eq. 3-12**, represented in **Eq. 3-8** - **Eq. 3-10**, are also affected by

the integration and application of orthogonality condition in **Eq. 3-12**. Also, M_{iq} and K_{iq}

are given as:

$$M_{iq} = \rho A\int_0^L \emptyset_{iq}^{(ii)}(x)dx \;;\; K_{iq} = EI\int_0^L \emptyset_{iq}^{(iv)}\emptyset_{iq}(x)dx \,;\, C_{iq} = 2\zeta_q\sqrt{M_{iq}K_{iq}} \qquad \textbf{Eq. 3-13}$$

In **Eq. 3-12** the impact of damping on the layered metamaterial structure is

considered. Here, C_{iq} and ζ_{iq} are the horizontal beam's damping coefficient and the

damping ratio of the i_{th} horizontal beam in q_{th} mode, respectively. The mode functions

of the fixed-fixed beams, $\emptyset_{iq}(x)$, are assumed to be the same as the trial function, $\emptyset_{iy}(x)$,

and given as [12]:

$$\emptyset_{iq}(x) = \emptyset_{iy}(x) = [sinh\beta_{iq}x - sin\beta_{iq}x + (\frac{sinh\beta_{iq}L - sin\beta_{iq}L}{cos\beta_{iq}L - cosh\beta_{iq}L})(cosh\beta_{iq}x - cos\beta_{iq}x)] \quad \textbf{Eq. 3-14}$$

Moreover, the wave number β_{iq} is given by:

$$cosh(\beta_{iq}L)cos(\beta_{iq}L) = 1 \qquad\qquad \textbf{Eq. 3-15}$$

Furthermore, using Newton's second law, the movement of each r_{th} local resonator on

each i_{th} horizontal beam (including the j_{th} horizontal beam) can be described as:

$$m_r\dot{Y}_{ir}(t) + f_d(x_r, t) + f(x_r, t) = 0 \qquad\qquad \textbf{Eq. 3-16}$$

Solving **Eq. 3-12** and **Eq. 3-16** simultaneously using Runge-Kutta numerical

method, the generalized displacements and the local resonator displacement are obtained.

The obtained resonator displacement is then substituted into **Eq. 3-2**, in order to obtain

the displacement of the horizontal beam. This Galerkin solution is truncated at N = 4.

Transmissibility is taken as the output displacement at the center of the uppermost

horizontal beam, i.e. $(x = \frac{L}{2})$, relative to the input vibration at the center of the lowest

horizontal beam, i.e., vibration source. This is obtained by substituting the generalized

displacement result, u_q, obtained from solving **Eq. 3-12** and **Eq. 3-16** simultaneously,

into **Eq. 3-2**. The transmissibility,η_T, is then given as:

$$\eta_T = \frac{w(0.5 * L, t)_{Beam\ i=j}}{w(0.5 * L, t)_{Beam\ i=1}} \qquad\qquad \textbf{Eq. 3-17}$$

3.2.2   <u>Single-Beam Model Analysis</u>

Conversely, to understand the difference in modelling between a single-beam

metamaterial structure and a layered-beam metamaterial structure, a simple of the Euler-

Bernoulli model of a single-beam structure is presented [12]. A representative design of a

single-beam metamaterial structure is shown in **Figure 3-4**. The structure is comprised of

a single horizontal beam and various local resonators attachments as shown in **Figure**

3-4. For the purpose of comparison, in analyzing the bandgap behavior of single-beam

metamaterial structure, the same material parameters used by Yu et al. [11] and Zhou et

al.[12] , Shown in **Table 3-1**, were used.
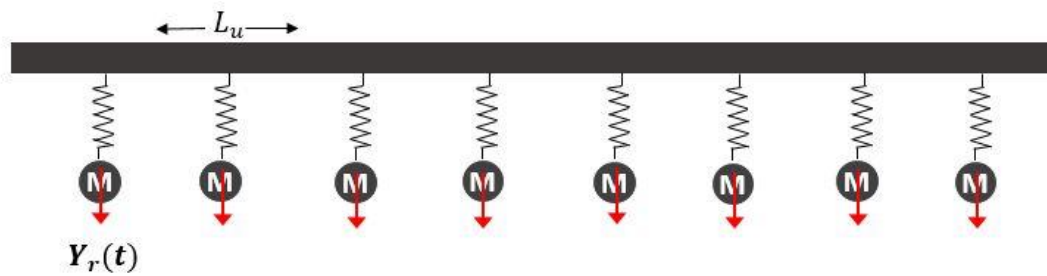
Figure 3-4: Schematic representation of a single-beam metamaterial structure.
M represents the mass of the local resonators, while $Y_r(t)$ is the displacement of the
local resonator.

Table 3-1: Model design parameters of the single-beam metamaterial structure and the layered-beam metamaterial structure used in comparative analysis.

Parameter	Value	Unit
Young's modulus of elasticity of the beam, E	70	GPa
Density of beam, ρ	2600	kg/m^3
Area of horizontal beam, A	1.602×10^{-4}	m^2
Area moment of inertia, I	5.968×10^{-9}	m^4
Modal damping ratio of horizontal beams, ζ_{ji}	0.02	
Vibration force magnitude, f_s	10	N
Length of unit cell beam, L_c	25	mm
Local resonator stiffness, k_r	1.65×10^5	N/m
Local resonator mass, m_r	0.0437	kg
Damping ratio of local resonators, ξ_r	0.01	
Length of Vertical Columns, l_c	80	mm
Width of Vertical column, b_c	7	mm
Thickness of Vertical Columns, h_c	5	mm
Damping ratio of vertical columns, ξ_c	0.02	

The displacement of the single-beam metamaterial structure in **Figure 3-4** can be

modeled with standard Euler-Bernoulli beam's equation in **Eq. 3-18** below [41]:

$$EI\frac{\partial^4 w}{\partial x^4} + \rho A\frac{\partial^2 w}{\partial t^2} = f_s(x,t)\delta\left(x - \frac{L}{2}\right) + \sum_{r=1}^{n} f(x_r,t)\delta(x - x_r) \qquad \textbf{Eq. 3-18}$$

where L, E and I still represent the total length of the horizontal beam ($L = \alpha * L_u$),

Young's elastic modulus and the cross-sectional moment of inertia of the horizontal

beam. Also, $f_s(x,t)$ and $f(x_r,t)$ in **Eq. 3-18** still represent the force from the vibration

source on the beam and the force from the local resonators, respectively.

The transverse displacement of the horizontal beam in **Eq. 3-18**, $w(x,t)$, can be

analyzed using Galerkin approach and superposition of mode shapes given in **Eq. 3-19**

below [12]:

$$w(x,t) = \sum_{q=1}^{N} u_q(t)\emptyset_q(x) \qquad \textbf{Eq. 3-19}$$

where u_q and $\emptyset_q$ in **Eq. 3-19** represent the generalized displacement and the trial of the

horizontal beam at the q_{th} mode, respectively. Furthermore, the displacement of the local

resonators is shown in **Eq. 3-20** below:

$$m_r\ddot{Y}_{qr}(t) + f_d(x_r,t) + f(x_r,t) = 0 \qquad \textbf{Eq. 3-20}$$

The expression $f_d(x_r,t)$ in **Eq. 3-20** represents the damping force of the local

resonator, while m_r is the mass of the local resonator. Also, Y_{qr} is the displacement of the

r_{th} local resonator in the q_{th} mode shape. The expressions of the forces in **Eq. 3-18** and

Eq. 3-19 are given below:

$$\begin{cases} f(x_r, t) = k_r[Y_r(t) - w(x_r, t)] \\ f_d(x_r, t) = 2\xi_r\sqrt{m_r k_r}\left[\dot{Z}_r(t) - \dot{w}(x_r, t)\right] \\ f_s = f_A \cos(\omega t) \end{cases} \quad \textbf{Eq. 3-21}$$

The expression f_A in **Eq. 3-21** represents the amplitude of the external vibration

force. Solving **Eq. 3-18** - **Eq. 3-20** simultaneously by substituting **Eq. 3-19** into **Eq.**

3-18, integrating through the length of the horizontal beam and applying orthogonality,

the transmissibility of the single-beam metamaterial structure can be obtained. The

expressions in **3-18 - Eq. 3-21** are also analyzed using Runge-Kutta numerical method.

3.3   Additional Models

To properly understand the behavior of the bandgap developed in the layered-

beam metamaterial structure, dispersion curve analysis is vital. COMSOL finite element

software and Eigen-Value equations are both used to develop two separate dispersion

curves in an attempt to predict the location of the bandgap expected from the layered-

beam metamaterial structure.

3.3.1   <u>COMSOL FE Model</u>

Next, COMSOL FEM software is used to investigate frequency bandgaps and

modes of vibrations. Afterwards, a theoretical model is developed from first principle

using Eigen-value equations and applied in investigating wave attenuation capabilities of

the presented metamaterial structure.

Figure 3-5 shows geometries and dimensions of the cantilever, i.e. the building

block of the metamaterial structure presented in this work and used for the COMSOL

model. First, a 3D CAD drawing of the unit cell was prepared using SolidWorks software

and the predetermined geometries and dimensions shown in **Figure 3-5**. The CAD

drawing was then imported into COMSOL finite element multi-physics software to

analyze the dynamic response of the metamaterial structure and also obtain the dispersion diagram that depicts the relationship between the wavenumber, $\mathcal{K}$, and frequencies for an infinite number of periodically arranged unit cells. That is, for an array of unit cells, at frequency intervals that meet Bragg's scattering condition, destructive interference occurs. This yields the desired frequency bandgap. The presence of the local resonators in the structure further enhances the frequency bandgap because at the resonant frequency of the locally resonating structures, the kinetic energy contained in the external vibrations is transferred to the local resonators; causing them to resonate while creating a lower frequency bandgap in the dispersion diagram of the metamaterial structure.

In the COMSOL model a fine mesh coupled with the choice of material properties (given in **Table 4-1**) and geometries (shown in **Figure 3-5**) are used to simulate the dispersion curve and obtain frequency bandgaps. The model assumes no damping effects and solves the governing equation of the metamaterial structure given by:

$$K_d = [K_u - \omega^2 M_u] \qquad\qquad \textbf{Eq. 3-22}$$

$$[K_u - \omega^2 M_u][q_L \ \ q_{int} \ \ q_R]^T = [F_L \ \ \mathbf{0} \ \ F_R]^T \qquad\qquad \textbf{Eq. 3-23}$$

where ω and K_d are frequency and dynamic stiffness matrix of the unit cell, respectively, and K_u and M_u are stiffness and mass matrices of the unit cell, respectively. Here, q_L, q_R, and q_{int} are displacement vector of the left side of the unit cell, displacement vector of the right side of the unit cell, and displacement vector of the internal nodes of the unit cell, respectively. Similarly, F_L and F_R are force vectors on the left and right sides of the unit cell, respectively. Upon finite element discretization, the unit cell contained 11,647 elements with a maximum size of 1.81 mm and a minimum size of 0.0775 mm.
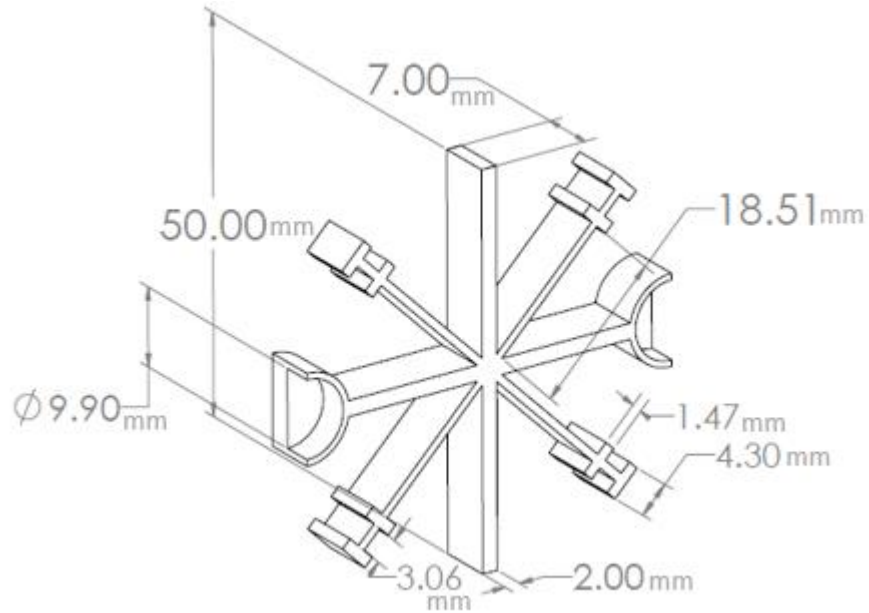
Figure 3-5: Metamaterial cantilever beams and central magnet used in COMSOL model simulations.

3.3.2   Eigen-Value Equation Model

Next, the layered-beam metamaterial structure is analyzed with the application of beam continuity theorem to Euler-Bernoulli beam with periodic arrangement of local resonators attached to the beam. This is shown in **Figure 3-6**. The method of transfer matrix is used in modelling the wave propagation across the beam, assuming small displacement of the beam [42].
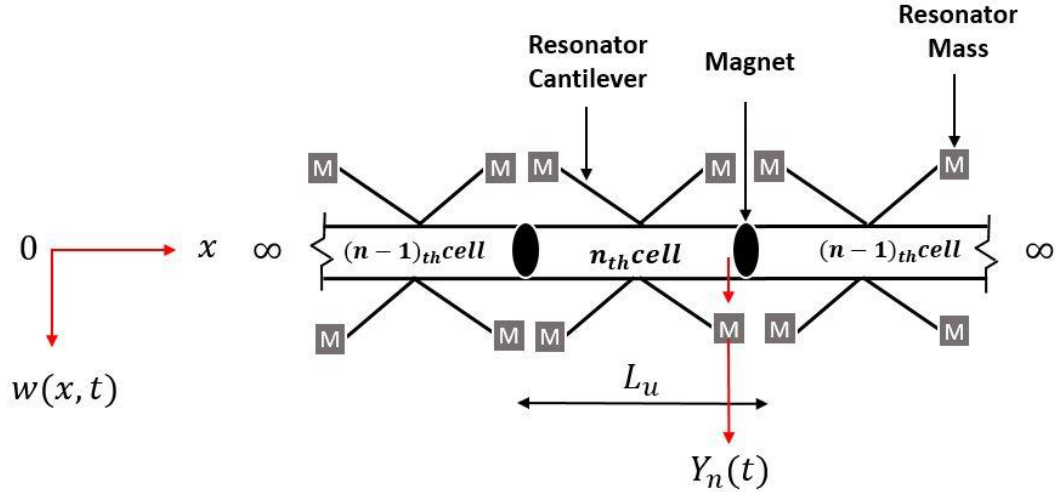
Figure 3-6: Cartoon model schematic of beam with local resonators showing the beam's continuity boundaries applied in developing the Eigen-Value equations.

The general equation of motion of the Euler-Bernoulli beam in **Figure 3-6** is given as:

$$EI\frac{\partial^4 w}{\partial x^4} + \rho A\frac{\partial^2 w}{\partial t^2} = 0 \qquad \textbf{Eq. 3-24}$$

For Eigen-value analysis, it is assumed that $w(x,t) = \emptyset(x)^{i\omega t}$, where $\emptyset(x)$ defines the mode shapes at point x, described as:

$$\emptyset(x) = Q\cos(\beta x) + B\sin(\beta x) + C\cosh(\beta x) + D\sinh(\beta x) \qquad \textbf{Eq. 3-25}$$

where β is the flexural wave number given as:

$$\beta^4 = \frac{\rho A\omega^2}{EI} \qquad \textbf{Eq. 3-26}$$

For the nth unit cell, the mode shape function can be rewritten as:

$$\emptyset_n(x') = Q_n\cos(\beta x') + B_n\sin(\beta x') + C_n\cosh(\beta x') + D_n\sinh(\beta x') \qquad \textbf{Eq. 3-27}$$

where $x' = x - nL_u$, $nL_u \leq x \leq (n+1)L_u$ .Here, $Q_n, B_n, C_{n,} and\ D_n$ are the unknown amplitudes describing the mode shape function [12].

The equation of the nth local resonator in **Figure 3-6** is described as:

$$F(x_n, t) + m\ddot{Y}_n(t) = 0 \qquad \text{Eq. 3-28}$$

where $F(x_n,t)$ is the force of the nth resonator developed as a result of interaction with the beam at the contact point as shown in **Figure 3-6**. Also, Y_n, is the vertical displacement of the mass of the resonator, m, during the external excitation. The force, $F(x_n, t)$, is given by:

$$F(x_n, t) = -k_r[y(x_n, t) - Y_n(t)]. \qquad \text{Eq. 3-29}$$

Assuming the solution for the vertical displacement of the mass resonator of the form:

$$Y_n(t) = V_n e^{i\omega t} \qquad \text{Eq. 3-30}$$

where V_n is the displacement of the local resonator (LR) and combining **Eq. 3-28** - **Eq. 3-30** yields:

$$m\ddot{Y}_n = k_r[y(x_n, t) - Y_n(t)] \qquad \text{Eq. 3-31}$$

Substituting Y_n and $y(x_n, t)$ into equation **Eq. 3-31** gives:

$$-m\omega^2 V_n e^{i\omega t} = k_r[\emptyset_n(0) - V_n]e^{i\omega t} \qquad \text{Eq. 3-32}$$

Re-arranging **Eq. 3-32** the vertical displacement, V_n, can be written as:

$$V_n = \frac{k_r \emptyset_n(0)}{(k_r - m\omega^2)} \qquad \text{Eq. 3-33}$$

Moreover, **Eq. 3-29** can be rewritten as:

$$F(x_n, t) = -k_r[\emptyset_n(0) - V_n]e^{i\omega t} \qquad \text{Eq. 3-34}$$

and substituting **Eq. 3-33** into **Eq. 3-34** yields:

$$F(x_n, t) = \frac{m\omega^2 k}{(k - m\omega^2)}\emptyset_n(0)e^{i\omega t} = F_n e^{i\omega t} \qquad \text{Eq. 3-35}$$

The model for the four unconnected resonators ($r = 1,2,3,4$) shown in **Figure 3-6**, at the interface with the beam can be derived as [24]:

$$F(x_n, t) = \frac{m\omega^2 k}{(k - m\omega^2)} \emptyset_n(0) e^{i\omega t} = F_n e^{i\omega t} \qquad \textbf{Eq. 3-36}$$

with the amplitude of displacement of the local resonators, V_n, given by

$$V_{n,r} = \frac{k_r \emptyset_n(0)}{(k_r - m_r \omega^2)} \ , \ r = 1,2,3,4 \qquad \textbf{Eq. 3-37}$$

Consequently, the force acting on the beam due to these four resonators can be obtained

from **Eq. 3-34** - **Eq. 3-35** and given by:

$$F(x_n, t) = \sum - (k_r[\emptyset_n(0) - V_{n,r}]) e^{i\omega t} = \sum \frac{m_r \omega^2 k_r}{(k_r - m_r \omega^2)} \emptyset_n(0) e^{i\omega t} = F_n e^{i\omega t} \ , \ r = 1,2,3,4 \qquad \textbf{Eq. 3-38}$$

Next, the continuity conditions at the point where the resonators meet the beam, as shown

in **Figure 3-6**, are imposed between the n_{th} unit cell and the $(n-1)_{th}$ cell. These include

displacement, slope, bending moment, and shear force and, respectively, given by:

$$\begin{cases} \emptyset_{n-1}(L_u) = \emptyset_n(0) \\ \emptyset'_{n-1}(L_u) = L'_n(0) \\ EI\emptyset''_{n-1}(L_u) = EI\emptyset''_n(0) \\ EI\emptyset'''_{n-1}(L_u) = EI\emptyset'''_n(0) - F_n \end{cases} \qquad \textbf{Eq. 3-39}$$

Substituting **Eq. 3-27** and **Eq. 3-38** into **Eq. 3-39** yields:

$$\psi_n = \mathcal{M}^{-1} U \psi_{n-1} \qquad \textbf{Eq. 3-40}$$

where $\psi_n = (Q_n, \ B_n, C_n, D_n)^T$. Here, U and $\mathcal{M}$ are given by:

$$U =$$

$$\begin{pmatrix} \cos\left(\left(\frac{\rho A \omega^2}{EI}\right)^{\frac{1}{4}} L_u\right) & \sin\left(\left(\frac{\rho A \omega^2}{EI}\right)^{\frac{1}{4}} L_u\right) & \cosh\left(\left(\frac{\rho A \omega^2}{EI}\right)^{\frac{1}{4}} L_u\right) & \sinh\left(\left(\frac{\rho A \omega^2}{EI}\right)^{\frac{1}{4}} L_u\right) \\ -\left(\frac{\rho A \omega^2}{EI}\right)^{\frac{1}{4}} \sin\left(\left(\frac{\rho A \omega^2}{EI}\right)^{\frac{1}{4}} L_u\right) & \left(\frac{\rho A \omega^2}{EI}\right)^{\frac{1}{4}} \cos\left(\left(\frac{\rho A \omega^2}{EI}\right)^{\frac{1}{4}} L_u\right) & \left(\frac{\rho A \omega^2}{EI}\right)^{\frac{1}{4}} \sinh\left(\left(\frac{\rho A \omega^2}{EI}\right)^{\frac{1}{4}} L_u\right) & \left(\frac{\rho A \omega^2}{EI}\right)^{\frac{1}{4}} \cosh\left(\left(\frac{\rho A \omega^2}{EI}\right)^{\frac{1}{4}} L_u\right) \\ -\left(\frac{\rho A \omega^2}{EI}\right)^{\frac{2}{4}} \cos\left(\left(\frac{\rho A \omega^2}{EI}\right)^{\frac{1}{4}} L_u\right) & -\left(\frac{\rho A \omega^2}{EI}\right)^{\frac{2}{4}} \sin\left(\left(\frac{\rho A \omega^2}{EI}\right)^{\frac{1}{4}} L_u\right) & \left(\frac{\rho A \omega^2}{EI}\right)^{\frac{2}{4}} \cosh\left(\left(\frac{\rho A \omega^2}{EI}\right)^{\frac{1}{4}} L_u\right) & \left(\frac{\rho A \omega^2}{EI}\right)^{\frac{2}{4}} \sinh\left(\left(\frac{\rho A \omega^2}{EI}\right)^{\frac{1}{4}} L_u\right) \\ \left(\frac{\rho A \omega^2}{EI}\right)^{\frac{3}{4}} \sin\left(\left(\frac{\rho A \omega^2}{EI}\right)^{\frac{1}{4}} L_u\right) & -\left(\frac{\rho A \omega^2}{EI}\right)^{\frac{3}{4}} \cos\left(\left(\frac{\rho A \omega^2}{EI}\right)^{\frac{1}{4}} L_u\right) & \left(\frac{\rho A \omega^2}{EI}\right)^{\frac{3}{4}} \sinh\left(\left(\frac{\rho A \omega^2}{EI}\right)^{\frac{1}{4}} L_u\right) & \left(\frac{\rho A \omega^2}{EI}\right)^{\frac{3}{4}} \cosh\left(\left(\frac{\rho A \omega^2}{EI}\right)^{\frac{1}{4}} L_u\right) \end{pmatrix} \qquad \textbf{Eq. 3-41}$$

$$\mathcal{M} = \begin{pmatrix} 1 & 0 & 1 & 0 \\ 0 & \left(\frac{\rho A\omega^2}{EI}\right)^{\frac{1}{4}} & 0 & \left(\frac{\rho A\omega^2}{EI}\right)^{\frac{1}{4}} \\ -\left(\frac{\rho A\omega^2}{EI}\right)^{\frac{2}{4}} & 0 & \left(\frac{\rho A\omega^2}{EI}\right)^{\frac{2}{4}} & 0 \\ -F & -\left(\frac{\rho A\omega^2}{EI}\right)^{\frac{3}{4}} & -F & \left(\frac{\rho A\omega^2}{EI}\right)^{\frac{3}{4}} \end{pmatrix} \qquad \textbf{Eq. 3-42}$$

respectively, and

$$F = \frac{1}{EI}\left(\sum \frac{m_r\omega^2 k_r}{(k_r - m_r\omega^2)}\right), r = 1,2,3,4 \qquad \textbf{Eq. 3-43}$$

From Bloch-Floquet's equation of period structures in the x-direction, we have:

$$\boldsymbol{\psi_n} = e^{izl_u}\boldsymbol{\psi_{n-1}} \qquad \textbf{Eq. 3-44}$$

Further, by letting $\mathcal{M}^{-1}\boldsymbol{U} = \boldsymbol{S}$ and substituting **Eq. 3-40** into **Eq. 3-44** yields:

$$\boldsymbol{S\psi_{n-1}} = e^{izl_u}\boldsymbol{\psi_{n-1}} \qquad \textbf{Eq. 3-45}$$

Eq. 3-45 can be further rearranged into a standard eigenvalue problem described by:

$$\left|\boldsymbol{S} - e^{izl_u}\boldsymbol{I}\right| = 0 \qquad \textbf{Eq. 3-46}$$

where $\boldsymbol{I}$ is a [4x4] identity matrix.

CHAPTER 4

FABRICATION AND EXPERIMENT METHODS

This chapter outlines the experimental procedure employed in validating the transmissibility results from the three different models. Section 4.1 discusses the detailed fabrication process for the 3-D prototype of the layered-beam metamaterial structure. Section 4.2 discusses the experimental setup used in collecting input and output displacement data applied in transmissibility analysis. Also, the experimental setup described was used in studying the power output from the layered-beam metamaterial structure. The contents of this chapter were fully adopted from two previously published journal articles: **1.** Winner Anigbogu, Hamzeh Bardaweel, "A Metamaterial-Inspired Structure for Simultaneous Vibration Attenuation and Energy Harvesting", Shock and Vibration, vol. 2020, Article ID 4063025, 12 pages, 2020. https://doi.org/10.1155/2020/4063025 and **2.** Anigbogu, Winner., Nguyen, Hieu., and Bardaweel, Hamzeh. "Layered Metamaterial Beam Structures With Local Resonators for Vibration Attenuation: Model and Experiment." Frontiers in Mechanical Engineering Vol. 7 (2021). https://doi.org/10.3389/fmech.2021.768508. Permission was obtained from all the co-authors involved in the published studies.

4.1   Fabrication

Figure 4-1 displays the design and concept of the metamaterial vibration attenuation energy harvesting system presented in this work. The metamaterial structure,

shown in **Figure 4-1**a, consists of repetitive design building blocks (unit cells). Each

design unit cell, shown in **Figure 4-1**b, contains four angled cantilevers with fixed-free

ends. A permanent magnet is placed in the center of each unit cell. The tip mass at the

free-end of each cantilever is made of copper coils wrapped around the free-end of the

cantilever as shown in **Figure 4-1**c. The coils serve two purposes: First, the coils form

additional mass to lower the resonant frequency of the vibrating cantilevers, thus,

lowering the frequency bandgap of the metamaterial structure. Second, the magnet-coil

system is used to extract electric energy from kinetic energy of the resonating cantilevers.
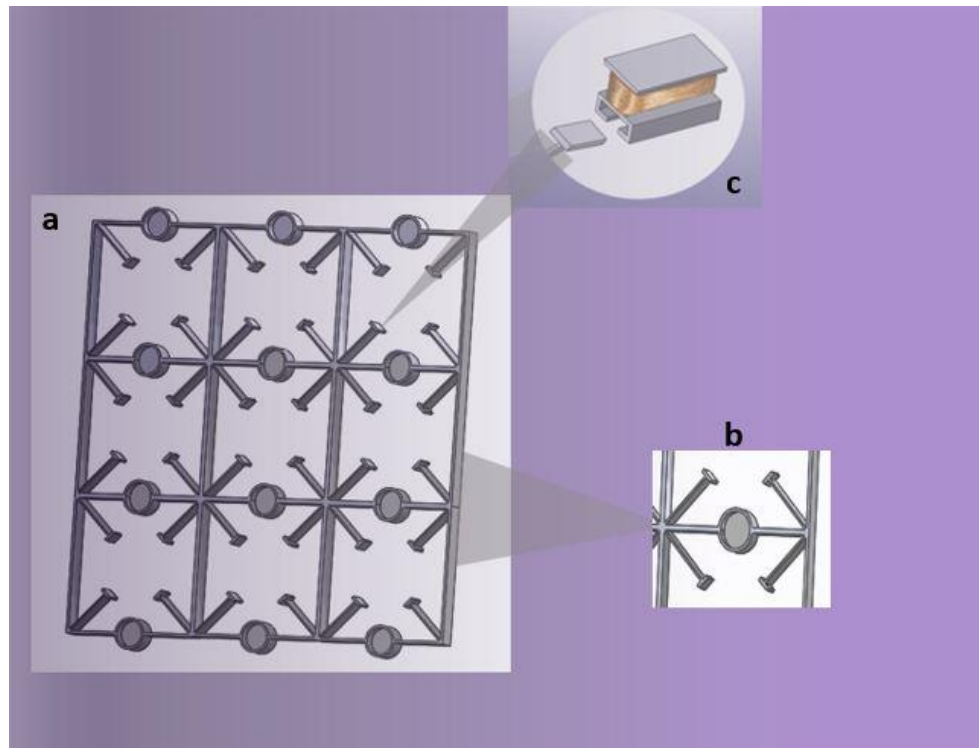
Figure 4-1: Concept and design of the metamaterial vibration attenuation energy harvesting structure presented in this work: a) Design layout of the metamaterial structure, b) Building block. Each design unit cell consists of four angled cantilevers and a central magnet mass, and c) The tip of each cantilever is made of insertion where copper coils are placed for power extraction.

The layered-beam metamaterial structure was designed using Solidworks CAD software, then changed into an STL (STereoLithography) format that is suitable for 3D printing. PETG (polyethylene terephthalate) was used as the printing filament in the Ultimaker 3 Fused Deposition Modeling (3D FDM) printer. The printed masses (cantilever beams) were designed in a way that allowed insertion of additional masses at their tips. The tip-masses were created separately and then slotted into the tips of the local resonators. Having the prospect of energy scavenging in mind, the tip-masses were made-up of 35 AWG enameled copper wires wound around the 3D printed masses. The number of turns was 220 and total length 9.04m. Also, small neodymium iron boron (NdFeB) permanent solid magnets were manually integrated into the horizontal beams of the 3D printed metamaterial structure. These additional tip-masses were vital in lowering the resonant frequencies of local resonators to less than 300 Hz. **Figure 4-2**. shows a prototype of the layered metamaterial vibration attenuation structure fabricated in this work. For this work, a layered metamaterial beam structure with four horizontal beams (j = 4) was chosen. This choice was informed by the need for the layered metamaterial structure to fit on the 3D printer bed used for fabrication. The dimensions and specifications of the manufactured layered metamaterial structure are outlined in **Table 4-1**.

Table 4-1: Design parameters of the layered metamaterial structure used to develop semi-analytical model.

Parameter	Value	Unit
Young's modulus of elasticity of the beam, E	2.7	GPa
Density of Beam, ρ	1270	Kg/m^3
Model Density Adjusted, ρ_{ad}	1100	
Length of Unit Cell Beam, L_u	50	mm
Width of Beam, b	7	mm
Thickness of beam, h	2	mm
Modal Damping ratio of Beam, ξ_q	0.02	
Vibration Force Magnitude, F_A	10	N
Mass of Resonator Tip, m_r	1.27	g
Length of Local Resonator, L_r	18.51	mm
Width of Local resonator, b_r	7	mm
Thickness of Local resonator, h_r	1	mm
Local Resonator Stiffness, k_r	745	N/m
Damping ratio of local resonators, ξ_r	0.01	
Length of Vertical Columns, l_c	50	mm
Width of Vertical column, b_c	7	mm
Thickness of Vertical Columns, h_c	2	mm
Damping ratio of vertical columns, ξ_c	0.02	
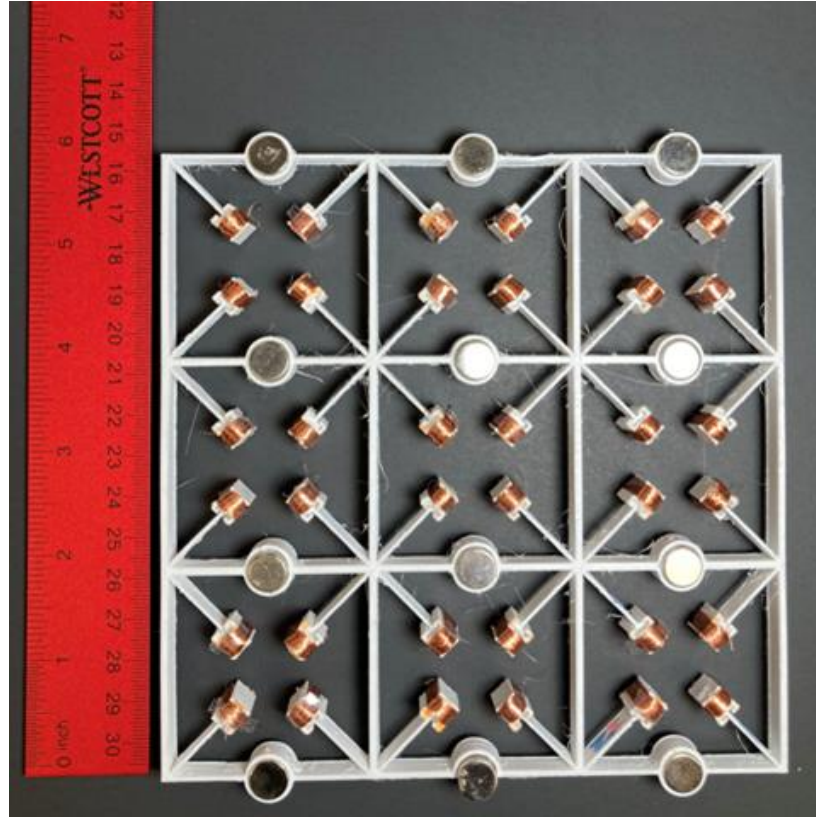
Figure 4-2: Figure 6: A 4x4 prototype of the manufactured layered metamaterial vibration attenuation structure presented and modeled in this work.

4.2   Experimental Setup

4.2.1   Transmissibility and Power Output Measurement

The set-up of the experiment is shown in **Figure 4-3**. First, an external vibration waveform was generated by the controller (S81B–P02, SENTEK DYNAMICS). This waveform was then passed through the power amplifier (LA-800, SENTEK DYNAMICS) for amplification, before reaching the shaker table (VT-500, SENTEK DYNAMICS). The electromagnetic shaker table was used to apply the external vibration input to the layered metamaterial structure that was fixed on top of the shaker table. The shaker table was operated at predetermined frequency range of 50 Hz to 700 Hz, and acceleration level of 0.5g [m.s−2]. The sides of the layered metamaterial vibration attenuation structure were

held with a fixture and clamps. Two accelerometers (PCB333B30 model, PCB Piezotronics) were used to capture the input signal from the shaker table and the output signal from the top of the layered metamaterial structure. The first accelerometer was placed on top of the shaker table to capture the input signal data, while the second accelerometer was positioned on top of the layered metamaterial structure to capture the output signal. The input and output signals were both monitored using Crystal Instrument's Engineering Data Management (EDM) software on a PC. The transmissibility was analyzed by comparing the output acceleration from the top-most beam of the metamaterial structure to the input acceleration from the vibration source, i.e., shaker table.

Additionally, the output voltage from a unit cell was measured across a load resistance and used to estimate the amount of recovered electric power. To measure the optimal load resistance of the coils at the tips of the resonators, the mid-frequencies of the first bandgap (i.e., 223 Hz) and the second bandgap (i.e., 615 Hz) were kept constant and the power output measured within a range of resistances (0 Ω to 1000 Ω). The varying resistances were chosen using the decade box shown in **Figure 4-3**.
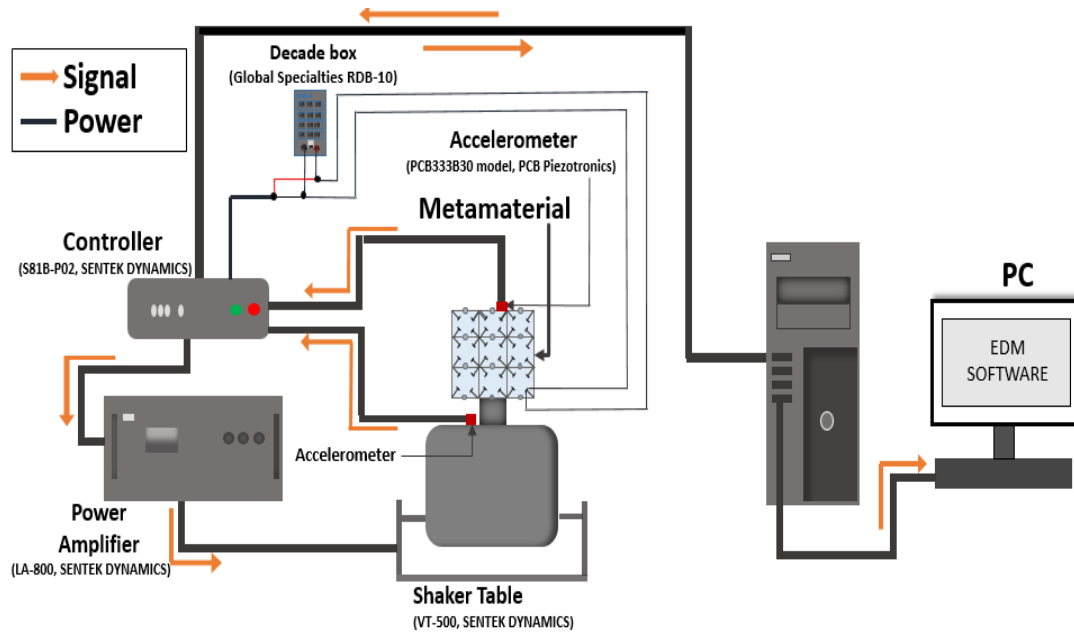
Figure 4-3: Cartoon schematic of the experimental set-up used for measuring the transmissibility of the layered metamaterial vibration attenuation structure presented in this work.

CHAPTER 5

RESULTS AND DISCUSSION

In this chapter the results of the models developed in Chapter 3 are presented. In section 5.1.1 of this chapter results of the dispersion curves' predictive analysis using COMSOL FEM model and Eigen-Value equations developed in Chapter 3 are presented. The ability of the two dispersion curves - which were developed through disparate modeling approaches - to predict similar bandgap regions is analyzed. Also in section 5.1.2 the results of the main semi-analytical model developed for modeling the transmissibility of layered-beam metamaterial structures are presented. Section 5.2 presents the results gathered from experimental data. Section 5.2.1 presents the experimental transmissibility result and compares it with the three models developed. Section 5.2.2 analyzes the ability of the layered-beam metamaterial structure to scavenge electricity using measured data from experiment. In section 5.3 the effects of variations in different design parameters of the layered metamaterial structure are presented. Lastly, section 5.4 presents the results of the comparative study between bandgap development in single-beam metamaterial structure and layered-beam metamaterial structure of the same sort. This chapter on results has contents derived previously published journal articles: **1.** Winner Anigbogu, Hamzeh Bardaweel, "A Metamaterial-Inspired Structure for Simultaneous Vibration Attenuation and Energy Harvesting", Shock and Vibration, vol. 2020, Article ID 4063025, 12 pages, 2020. https://doi.org/10.1155/2020/4063025

and **2.** Anigbogu, Winner., Nguyen, Hieu., and Bardaweel, Hamzeh. "Layered Metamaterial Beam Structures With Local Resonators for Vibration Attenuation: Model and Experiment." Frontiers in Mechanical Engineering Vol. 7 (2021). https://doi.org/10.3389/fmech.2021.768508. Permission was obtained from all the co-authors involved in the published studies.

5.1 Model Validation

5.1.1 Dispersion Curve Analysis

COMSOL Dispersion Curves and Unit-Cell Displacement

To fully understand the behavior of the presented metamaterial vibration attenuation energy harvesting structure, we further analyze the results of the COMSOL FEM model described in section 3.3. The frequency bandgaps of the metamaterial vibration attenuation energy harvesting structure shown in **Figure 5-1** are analyzed using COMSOL FEM. Periodic boundary conditions were imposed and geometric and material properties were set similar to those measured and reported in **Table 4-1**. **Figure 5-1** shows the dispersion curve of the metamaterial structure obtained using COMSOL model described in section 3.3. **Figure 5-1** suggests that there exists two major bandgaps within frequency range of 100-1000 Hz. The first and second bandgaps are 218-247 Hz and 589-780 Hz, respectively.
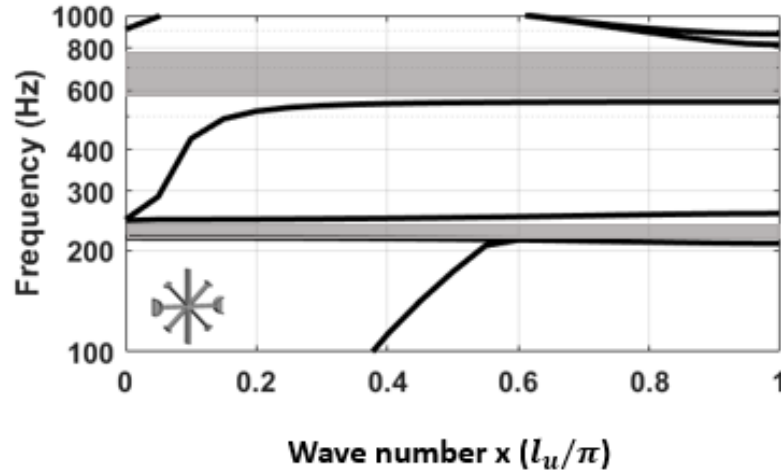
Figure 5-1: Dispersion curve and frequency bandgaps of a metamaterial structure consisting of cantilever beams with tip coils and central magnet obtained using COMSOL simulations. Frequency bandgaps: The first and second bandgaps are 218-247 Hz and 589-780 Hz, respectively, (marked in gray).

Figure 5-2 shows the corresponding mode shapes obtained using COMSOL at the

lower and upper edges of the first and second bandgaps, i.e. 218, 247, 589, and 780 Hz,

respectively. Clearly, within these bandgaps vibrations are attenuated and trapped within

the metamaterial structure. Also, the fundamental resonant frequency of the unit cell

(combined cantilever beams, tip coils, and central magnet) was estimated using

COMSOL at approximately 224 Hz. The fundamental resonant frequency falls within the

first bandgap of the metamaterial structure, i.e. 218-247 Hz. As shown in **Figure 5-2**, at

the lower and upper edges of the first bandgap, the deformations of the unit cell are

localized within the cantilevers. The vibrational energy is localized within the frequency

bandgap and converted into kinetic energy of the resonating cantilevers. Also, **Figure 5-2**

suggests that maximum bending deformations of the local resonators occur within the

first bandgap. Therefore, it is expected that most of energy harvesting will occur within

the first bandgap. This observation agrees with the vibration energy harvesting

measurements that were performed in this work and discussed later in this article. Since

most mechanical vibrations in nature occur at frequencies lower than 300 Hz [14], in this work, energy harvesting is targeted within this bandgap, i.e. 218-247 Hz.
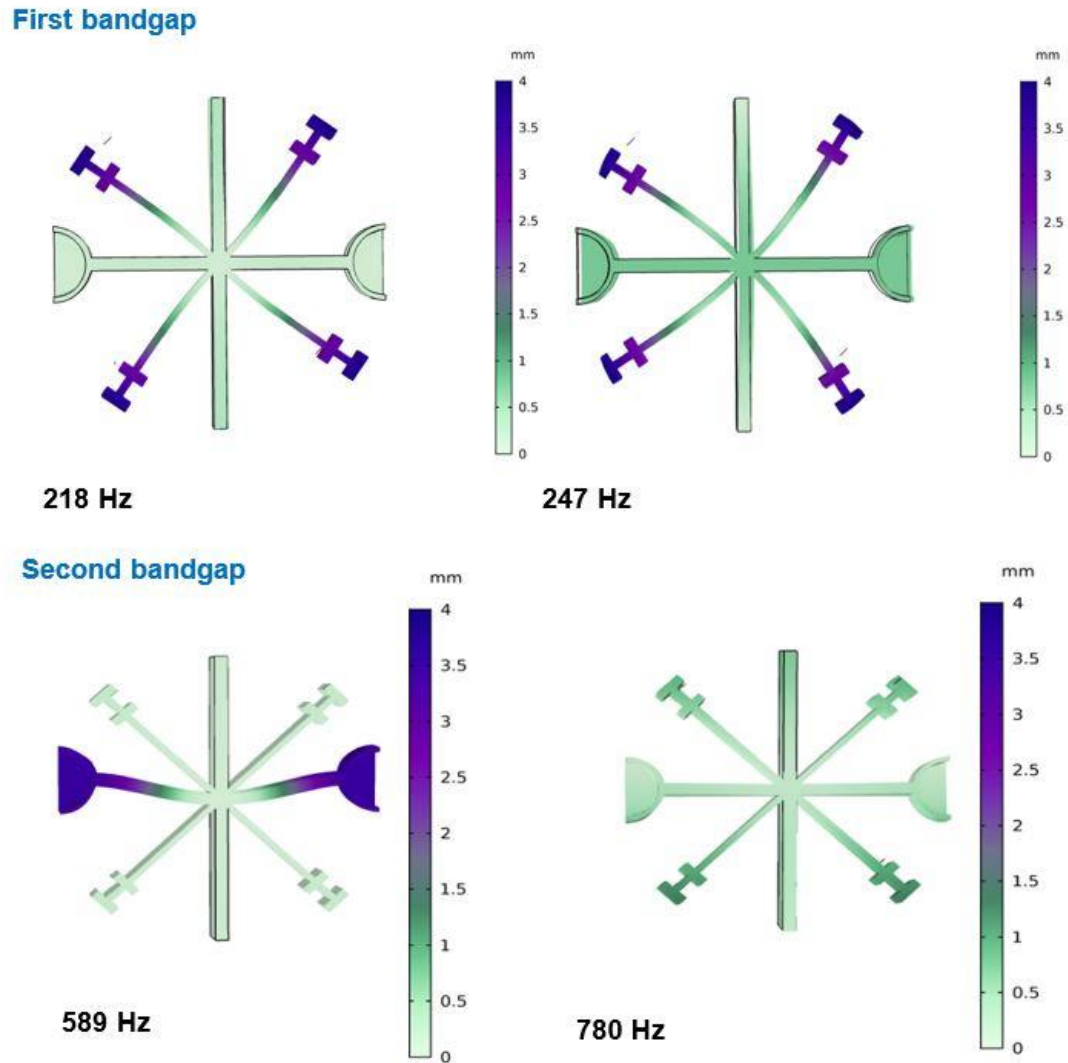
Figure 5-2: Mode shapes at the edge frequencies of each bandgap obtained using COMSOL model simulations.

Eigen-Value Equation Dispersion Curve Result

Moving a step further in confirming the COMSOL FEM dispersion curve result, wave propagation through the metamaterial structure is investigated using the Eigen-value equation developed in **Eq. 3-46**. For every selected frequency value, ω, the

solutions of the wave vector, z , are obtained. **Figure 5-3** shows the results obtained

from solving the eigenvalue problem given by **Eq. 3-46**. Here, a stop-band exists when z

is imaginary, while a pass-band exists when z is real [12]. As shown in **Figure 5-3**, the

stop-bands of the wave are marked in gray. Results reveal that there exists two main stop-

bands in the frequency range 1-1000 Hz. These bands are occurring in the range of 121-

310 Hz (lower frequency range) and 528-674 Hz (higher frequency range), respectively.

These two bands are the result of the horizontal-beam itself and the Local resonators (LR)

[23]. That is, a higher frequency stop-band is created as a result of vibration phase

differences – in phase and out of phase - between adjacent unit cells. A low frequency

stop-band is typically generated by the LR stop-band due to the attenuation effect of the

resonators.
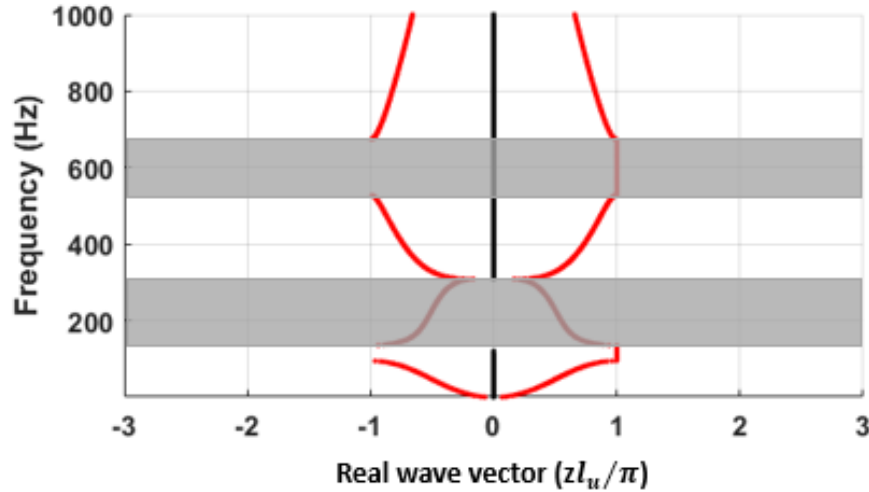
Figure 5-3: Band structure obtained by solving **Eq. 3-46** to investigate the wave attenuation capabilities of the metamaterial structure. First and second frequency bandgaps are 121-310 Hz (lower frequency range) and 528-674 Hz (higher frequency range), respectively, (marked in gray).

5.1.2   Semi-Analytical Model Results

Having obtained the dispersion curves of the layered-metamaterial structure

showing the possible positions of bandgaps, the transmissibility of the layered-beam

metamaterial structure is then presented with FRF. The results from the FRF analysis

were obtained from **Eq. 3-17** as the Root Mean Square ratio between the output

displacement (at the center of the uppermost beam) and the input displacement (from the

vibration source) [12]. The parameters used in this study are shown in **Table 4-1**. For the

purpose of model validation and design investigation, a layered metamaterial structure

made of 3 unit cells per horizontal beam, three vertical columns between beams, and a

total of four horizontal beams was manufactured (**Figure 4-2**). The size limitation of the

3D-printer used in this research work informed our decision to focus on 3 unit cells per

beam and four horizontal beams. In this study, modes beyond the fourth modes were

truncated because higher modes are unnecessary as have been shown in the literature

[14]. For example, the 5th mode of the unit cell is 1469 Hz, which is much higher than the

frequency range of interest in the current study (below 700 Hz). When frequencies much

higher than 700 Hz are considered, the value of N should be increased to capture those

higher modes [12].

We start by examining the displacement amplitude of the topmost local resonator,

i.e., cantilever beam, and the lowest local resonator. Displacement response was

obtained using **Eq. 3-16** and results are shown in **Figure 5-4**. Results reveal peak

displacement at approximately 220 Hz. This peak closely corresponds to the first

fundamental resonant frequency of the unit cell which was also determined and verified

using COMSOL simulations and found at, approximately, 224 Hz [34].
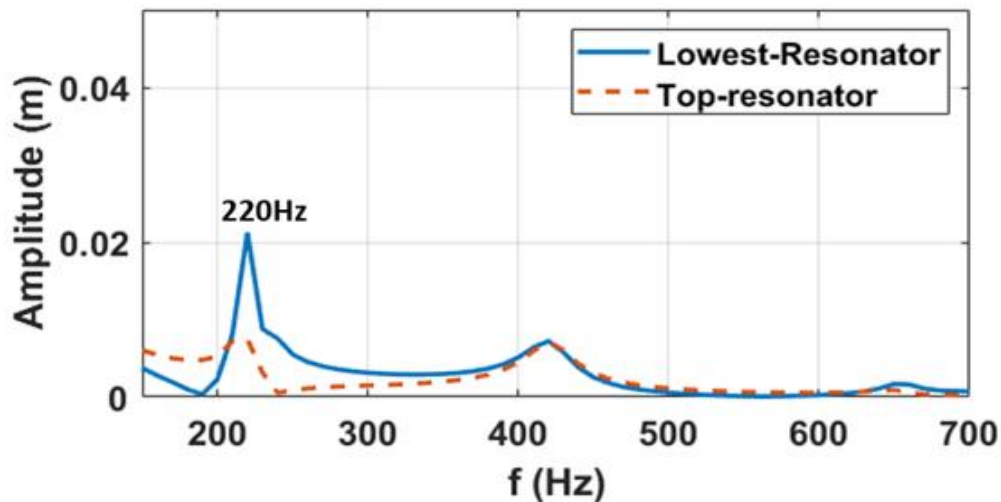
Figure 5-4: Displacement amplitude of local resonators at the top horizontal beam and the lowest horizontal beam showing resonant peak around 220 Hz, close to the overall resonant peak of the unit cell, F_n=224 Hz.

Next, the transmissibility of the metamaterial structure was estimated using **Eq. 3-17** and the results are shown in **Figure 5-5**. Results reveal two main bandgaps of

interests, i.e., below 700 Hz. Frequencies higher than 700 Hz were not considered in this

work because most of mechanical vibrations in nature occur at frequencies well below

the 700 Hz frequency limit adopted in this work [14]. The first bandgap expands from

190 Hz to 410 Hz with its lowest transmissibility dip occurring at approximately 245 Hz.

The second frequency bandgap takes place between 550 Hz - 710 Hz with its lowest dip

at approximately 600 Hz.
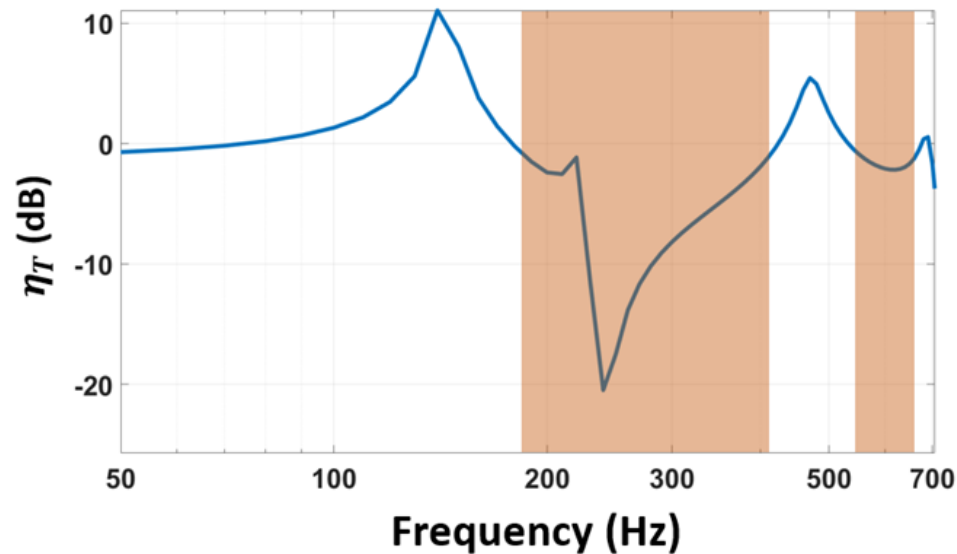
Figure 5-5: Transmissibility of the layered metamaterial vibration attenuation structure
obtained using model simulations. The first bandgap (190 Hz – 410 Hz) and the second
bandgap (550 Hz – 710 Hz) are shown in the shaded regions.

It is worth noting that the level of vibration attenuation, shown in **Figure 5-5**,

observed within the first bandgap is significantly larger than the level of vibration

attenuation observed in the second bandgap. This is likely because most of the vibrational

energy is localized within the first bandgap. To further investigate this behavior, the input

and output displacements of the layered metamaterial structure at frequency within the

first bandgap, F_n= 224Hz, are obtained using **Eq. 3-12** and **Eq. 3-2**. Results are shown in

Figure 5-6a. Similarly, output and input displacements are obtained at higher frequency

within the second bandgap, i.e., 600 Hz using **Eq. 3-12** and **Eq. 3-2** and results are shown

in **Figure 5-6**b. **Figure 5-6**(a-b) reveals that, at those selected frequencies, the output

displacement amplitudes are suppressed compared to the input displacement amplitudes.

Nonetheless, near the fundamental resonant frequency of the cantilever, i.e., 224 Hz the

vibrations are trapped in the local resonators. This localization of vibrational energy

results in significant reduction in the displacement of the most-upper beam (output)

compared to the bottom beam near the vibration source (input) as shown in **Figure 5-6**a.

This observation explains the substantial dip in transmissibility within the first bandgap

compared to the second bandgap as shown in **Figure 5-5**.
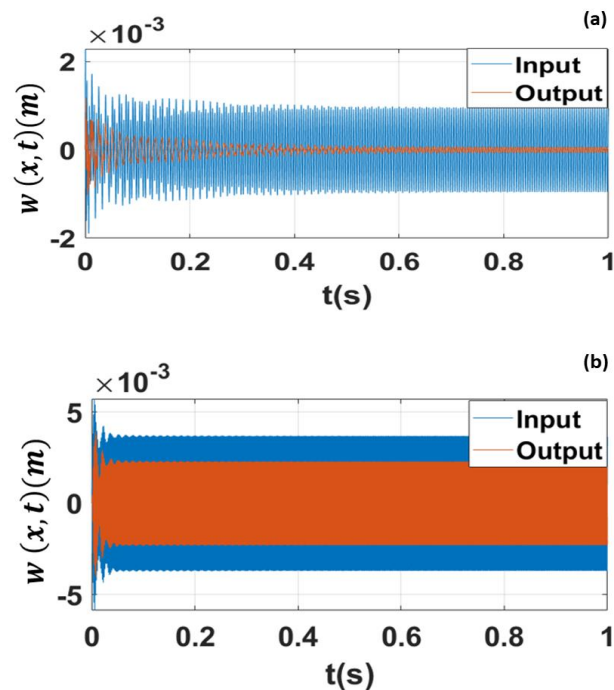
Figure 5-6: Model simulations of displacement response of the local resonators at the topmost beam and the lowest beam within the two main frequency bandgaps: **(a)** within the first bandgap at the unit cell's resonant frequency, F_n=224 Hz, **(b)** within the second bandgap, F=600 Hz.

5.2   Experimental Results

5.2.1   <u>Transmissibility Result</u>

In this section, model simulations are validated against experimentally measured

data and the results are shown in **Figure 5-7**. Measured data shown in **Figure 5-7** were

obtained using experimental setup shown in **Figure 4-3**. Results show a good agreement

between model simulations and measured data (**Figure 5-7**). While results from both

model simulations and experimental data exhibit alike characteristics and trends some

discrepancy is present. For example, semi-analytical model simulations predict a second

bandgap of 550 Hz – 710 Hz compared to the measured one, i.e., 587-639 Hz. This

mismatch between model simulations and measured data may be attributed to a few

factors. First, the mismatch between model simulations and experimental data may be

attributed to the protrusions and cuts that exist in the fabricated layered-beam

metamaterial structure and were not factored into the model simulations. The presence of

some extruded cuts and holes in the 3D printed layered metamaterial structure, coupled

with defects accrued from assembling the tip masses and the 3D printed layered

metamaterial structure may contribute to the slight mismatch between model and

experiment. Second, printing parameters such as temperature, extrusion rate and speed

may affect the quality of 3D printed structures [14], [43]–[47]. These are factors that

cannot be readily accounted for in the developed model. For example, Reichl et al., found

that changes in 3D printing temperature may affect the damping properties of cantilever

vibration absorbers and therefore likely to adjust their resonant frequencies [43]. In this

work, similar to the approach taken by Xia et al., fixed modal damping ratio was assumed

for simplicity [1]. Additionally, the slight mismatch between model simulations and

experiment may be attributed to the experimental setup itself. For instance, deviation between dynamic model predictions and experiment was reported by Dong et al. [41], Lee et al. [48], Berdy et al. [49], and Dhote et al. [50] and it was attributed to the likely presence of a small tilt in the experimental rig which may lead to multi-direction vibrations and damping that are not accounted for in the dynamic model.
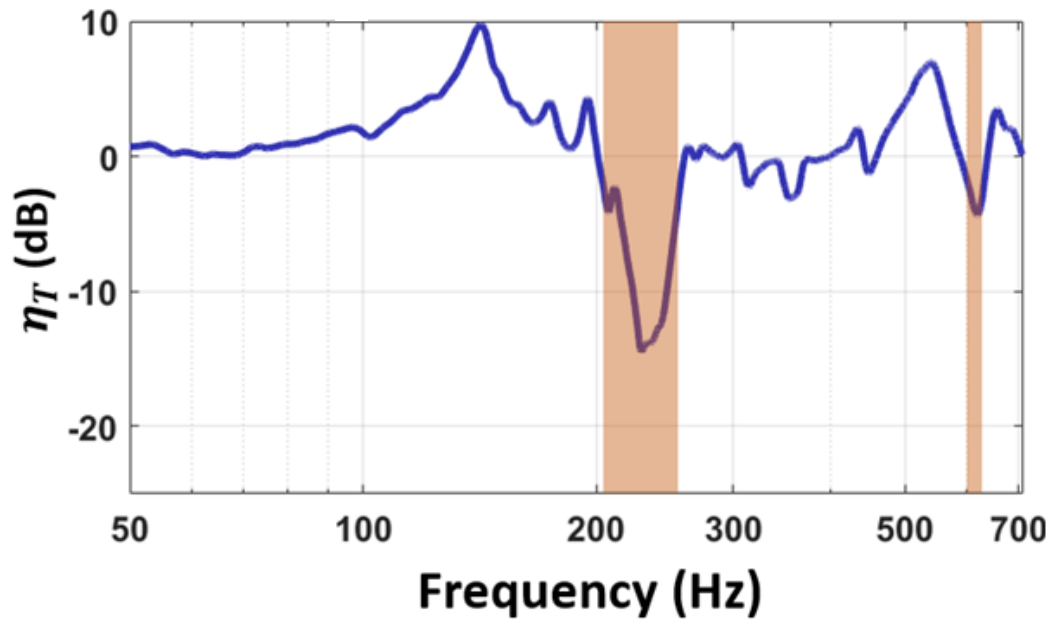
Figure 5-7: Measured transmissibility of the layered metamaterial vibration attenuation structure showing two notable frequency bandgaps, i.e., 205-257 Hz and 587-639 Hz

Results from COMSOL model simulations and Eigen-value equation (**Eq. 3-46**) also show good agreement between models' predictions and measured experimental data (**Figure 5-7**) for both bandgaps. However, some discrepancy between models' predictions and measured data is still evident. The measured bandwidth of the first bandgap (205-257 Hz) is wider than the bandwidth of the COMSOL simulation-based first bandgap. A similar observation was made and reported by Chen et al. [14]. This may be attributed to some of the approximations made in the COMSOL model simulations

including absence of damping [14]. Similarly, the first bandgap obtained from **Eq. 3-46** is a little wider than the bandgap predicted by COMSOL simulations and experiment as shown in **Table 5-1**. This is likely because of some of the simplifications and approximations made in the model (**Eq. 3-46**) including absence of damping. Also, the Eigen-value equation model does not factor in some of the experimental design complexities including the flange attachment at the contact point with the beam. The model also assumes small displacements of the transverse beam and ignores the mass contribution from the transverse beam. Nonetheless, both models predict similar behaviors and show alike trends compared to measured data. The two main transmissibility regions are clearly in agreement for all models and experiment. Furthermore, results from experiment show that the level of vibration attenuation, represented as the dip in the transmissibility curve in **Figure 5-7**, occurring in the first bandgap is substantially larger than the level of vibration attenuation observed in the second bandgap. This behavior is expected since, as discussed earlier and shown in **Figure 5-2**, the second bandgap experiences less deformations compared to the first bandgap and most vibrational energy is localized within the first bandgap where the fundamental resonant frequency is located, i.e. 224 Hz. In **Table 5-1** below, the frequencies ranges of the first and second bandgaps for the three model approaches and experiment are presented in a tabular form.

Table 5-1 Comparison between frequency bandgaps obtained using experiment and models.

	Experiment	COMSOL simulations	Eigen-value equation	Semi-analytical model
First band (Hz)	205-257	218-247	121-310	190 – 410
Second band (Hz)	587-639	589-780	528-674	550 – 710

5.2.2   Energy Scavenging Capability Analysis

The ability of the fabricated layered-beam metamaterial structure to scavenge electric power while concurrently attenuating undesired vibrations is examined next. **Figure 5-8** shows electric power harvested from one cantilever located in the bottom central unit cell of the metamaterial structure. In this experiment the metamaterial structure was driven harmonically at 0.5g m.s-2 and fixed frequency (selected within the first bandgap, i.e. 223 Hz) while the load resistance was swept in the range of 1-1000 Ω (**Figure 5-8**a). The same experiment was repeated at a fixed frequency selected from the second bandgap, i.e. 615 Hz, as shown in **Figure 5-8**b. Results from these experiments confirm that most of the vibrational energy is localized within the first bandgap; causing the cantilevers to locally resonate. Consequently, within the first bandgap, kinetic energy in these resonating cantilevers is effectively converted into electric power through the coils at the free-end of these cantilevers. Maximum power outputs of, approximately, 2.5 µW and 0.6 nW were measured at 223 Hz (first bandgap) and 615 Hz (second bandgap), respectively. Thus, results demonstrate that both vibration transmissibility (**Figure 5-7**) and energy harvesting (**Figure 5-8**) characteristics of the fabricated metamaterial

structure are more prominent in the first frequency bandgap. Also, **Figure 5-8** reveals that the maximum power output occurs at optimum load resistance of 15 Ω.
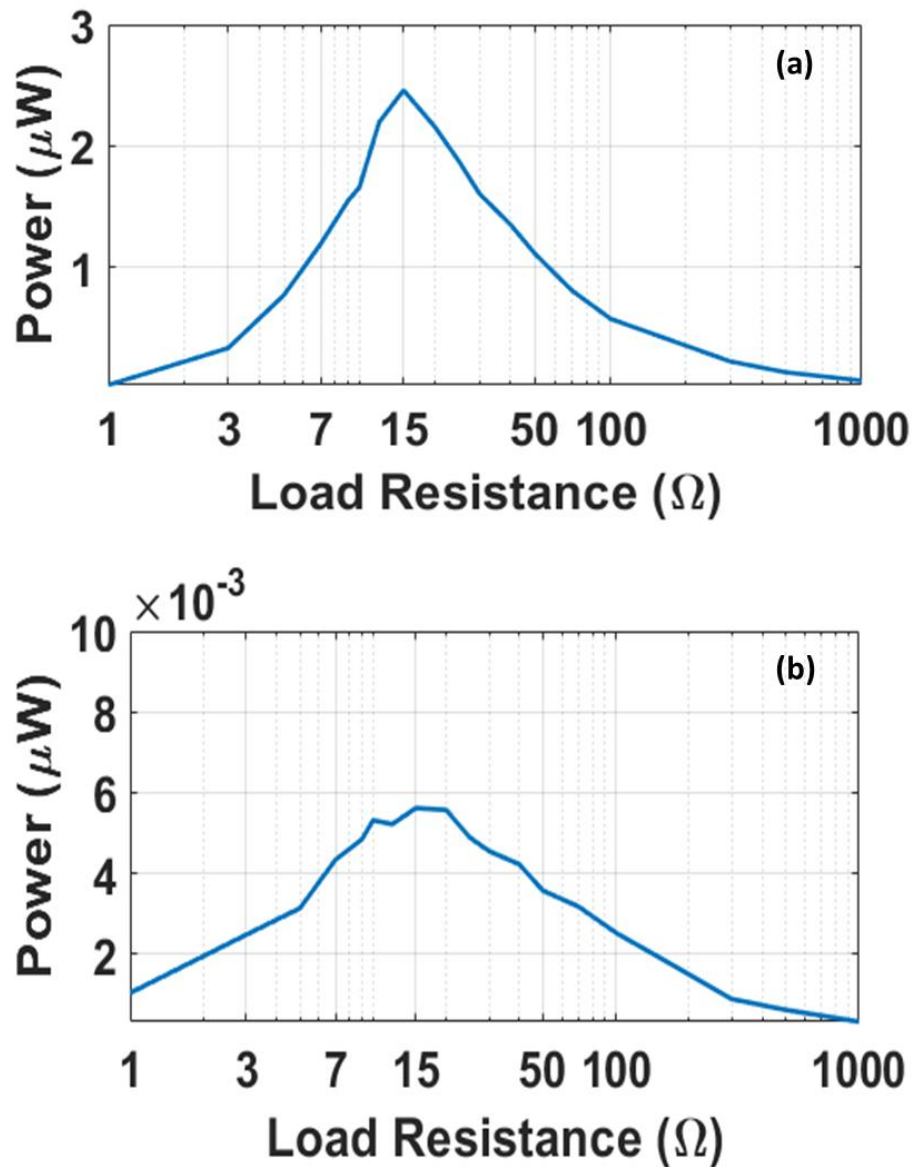
Figure 5-8: Measured electric power from a single cantilever within a unit cell at (a) 223 Hz and (b) 615 Hz and 0.5g m.s-2.

It is also worth noting that the improvement in energy harvesting within the first bandgap (205-257 Hz) is accompanied by stronger vibration attenuation. That is, vibration attenuation and energy harvesting characteristics of the metamaterial structure

are coupled. Stronger vibration attenuation leads to enhanced vibration energy harvesting capabilities. This is further demonstrated in **Figure 5-9** which shows the output electric power versus frequency. In this experiment, the metamaterial structure was swept harmonically at 0.5g m.s-2 in the frequency range of 50-500 Hz. The load resistance was fixed at the optimum value, i.e. 15 Ω, in order to maximize power generation. It is clear that, within the bandgap (205 Hz-257 Hz), the large dip in the transmissibility curve (**Figure 5-7**) corresponds to the maximum power generation (**Figure 5-9**). Also, **Figure 5-9** reveals that the maximum power generated within the frequency bandgap can reach up to, approximately, 5.2 µW at 245 Hz.
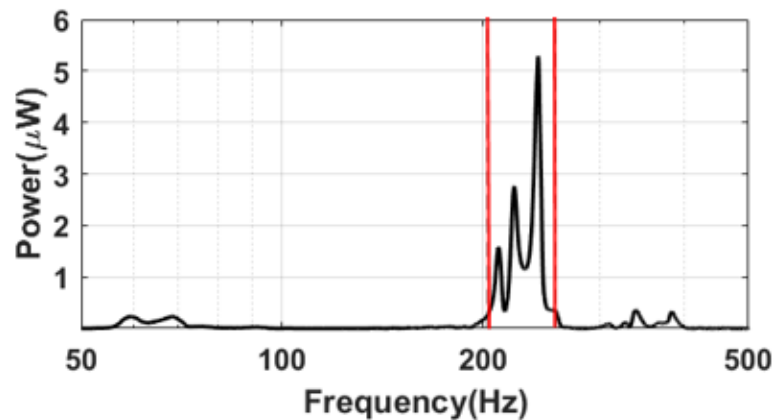
Figure 5-9: Measured output electric power spectrum from a single cantilever at fixed, optimum, load resistance of 15 Ω and acceleration level of 0.5g m.s-2. Measured frequency bandgap is denoted in red.

It is important that performance metrics of the presented metamaterial vibration attenuation energy harvesting structure are compared to the state-of-the-art work reported in recent literature. This is shown in **Table 5-2**. The fabricated metamaterial vibration attenuation energy harvesting structure performed very well compared to other efforts recently reported in the literature. For example, the metamaterial structure was able to

attenuate undesired vibrations at the, typically, targeted frequencies, i.e. less than 300 Hz. Concurrently, the presented metamaterial structure produced significantly more electric power compared to what has been reported in the literature. **Table 5-2** also shows another advantage of the work presented in this article. The optimum load resistance to maximize electric power was significantly lower compared to what has been reported in the literature. This low impedance guarantees higher electric current that is desirable to operate electronic circuits for sensors, as discussed earlier in this article. Although our initial prototyping efforts produced a metamaterial structure with comparable metrics to what has been reported in the literature, it should be noted that optimization of this metamaterial dual-purpose structure is beyond the scope of work reported in this article. The work reported in this article is focused on design, proof-of-concept experiments, and characterization tests of the metamaterial structure rather than optimization. Several design improvements can be made to improve the overall performance of the fabricated metamaterial dual-function structure. This includes optimization of geometries and dimensions of the cantilever beams, tilt angle of cantilever beams, number of unit cells, and size and location of central magnets, etc.

Table 5-2: Comparison between power output and load resistance of presented work with recent advancements in the field.

	Load Resistance (KΩ)	Power Output (μW)	First frequency bandgap (Hz)	Specifications
Ying Li et al.[14]	1,000	0.05	146-171	Simultaneous vibration attenuation and energy harvesting using Piezoelectric, PVDF.
Jung-San Chen et al.[37]	200	0.5	340-426	Simultaneous vibration attenuation and energy harvesting using Piezoelectric, PVDF.
Xu et al. [51]	-	-	144-188	Only vibration attenuation.
Zhu et al. [52]	-	-	210-700	Only vibration attenuation.
Kyung Ho Sun et al. [53]	20	0.345	-	Only energy harvesting capability using acoustic metamaterial and a double-clamped piezoelectric bimorph plate. Results were reported at 600 Hz.
This work	0.015	5.2	205-257	Simultaneous vibration attenuation and energy harvesting using magnet-coil system.

5.3 Dynamic Behavior of Layered Metamaterial Structures

5.3.1 Effects of Varying Parameters on Transmissibility

Effect of Increase in Resonator Number per Beam

Furthermore, design criteria and effects of different design parameters on the response of the layered metamaterial vibration attenuation structure are investigated using the developed semi-analytical model. **Figure 5-10** shows the effect of the number of local

resonators (unit cells) per beam on the transmissibility of the layered metamaterial

structure. It is worth noting that each unit cell has a length, L_u= 50mm and one local

resonator. The nominal original horizontal beam is comprised of three-unit cells,

implying three local resonators per beam. Therefore, an increase in the number of local

resonators (unit cells) per horizontal beam from 3 to 5 yields an increase of the overall

length of all the horizontal beams (L) from 150mm to 250mm (**Figure 5-10**a). **Figure

5-10**b shows that an increase in the number of local resonators (unit cells) per beam leads

to new frequency bandgaps opening up at lower frequencies. For instance, increasing the

number of resonators from 3 to 5 introduces a new bandgap at lower frequencies i.e., 98

Hz – 128 Hz. The same pattern of an extra bandgap opening up at lower frequencies

persists when the local resonators increased to 7 and then 10. This is likely because, with

an increase in the number of unit cells, more resonant peaks are expected to appear at

lower frequencies [12]. Also, an increase in the number of local resonators means that the

length of the horizontal beams and the forces acting on these beams are changed while

the geometry of the local resonators remained the same. Therefore, in **Figure 5-10**b, the

new bandgaps can also be attributed to Bragg's scattering that is resulting from intrinsic

changes on the horizontal beam. It can also be observed that the depth of the bandgap

decreased when the number of local resonators increased. This reduction in the depth of

the transmissibility is likely due to the fact that, with an increase in the number of local

resonators, there is also a concurrent increase in the number of vertical beams holding the

horizontal beams. The increase in the number of vertical beams makes the overall layered

metamaterial vibration attenuation structure stiffer; resulting in smaller transmissibility

depths as shown in **Figure 5-10**b. Therefore, a tradeoff between having more bandgaps at

lower frequencies and reduction in the transmissibility dips exists.
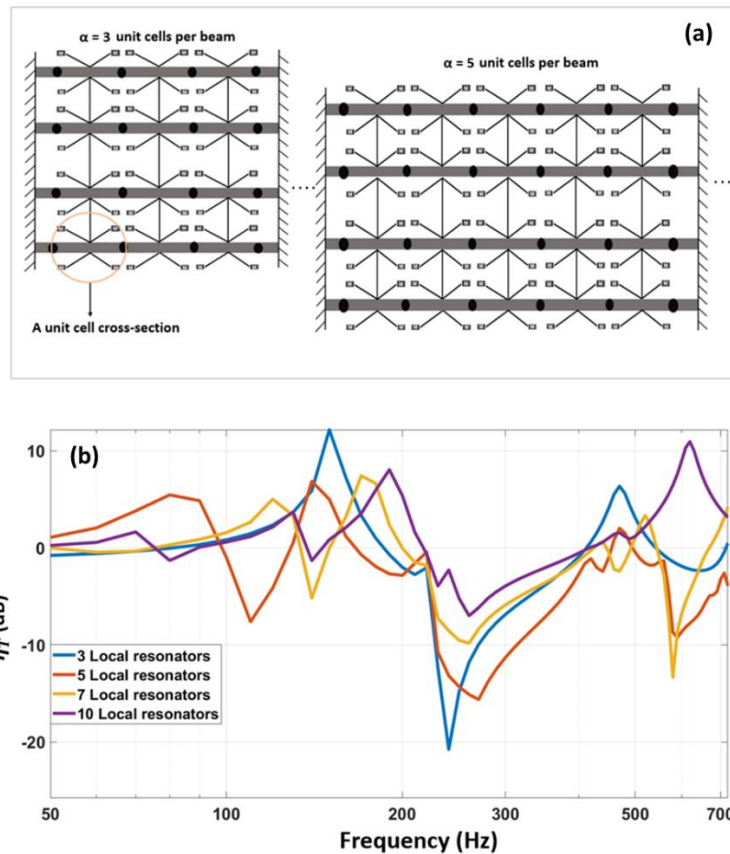
Figure 5-10: Effect of increasing the number of local resonators (unit cells) on the
transmissibility behavior of the layered metamaterial vibration attenuation structure:
(a) Graphical cartoon representation of changes in the layered metamaterial structure
as the number of unit cells (local resonators) per beam increases from α = 3 to α = 5.
(b) Model simulation of transmissibility when increasing the number of local
resonators.

Effects of Variation in Resonator Length

The impact of changes in the local resonators design on the first frequency

bandgap is properly analyzed. The lengths of the resonators are varied and results are

shown in **Figure 5-11**. Results show that increasing the length of the local resonators

causes the first bandgap to move to lower frequencies. Results also suggest that when the

length of the local resonators is increased above the nominal length, L_r, the high

frequency bandgap, i.e., second frequency bandgap, stays almost unchanged. For instance, when the length of the local resonators is increased from $1.5L_r$ to $1.8L_r$ the first bandgap shifts from 118 Hz - 250 Hz to 93 Hz - 200 Hz while the second frequency bandgap remains the same i.e., 440 Hz - 660 Hz. This is likely because an increase in the length of the local resonator reduces the stiffness and subsequently its resonant frequency; causing the first bandgap to shift to lower values. The second bandgap remains unchanged because it is mostly affected by the dimensions of the horizontal beams which remained fixed. This is because higher frequency bandgaps are mostly affected by vibration phase differences between adjacent unit cells [23]. When the dimensions of the horizontal beam are not changed the higher frequency bandgap is minimally impacted. The transmissibility dip of the first bandgap, when the length of the local resonator is changed to $1.8L_r$, falls within the region of the new resonant frequency, F_n= 105 Hz, of the local resonator.
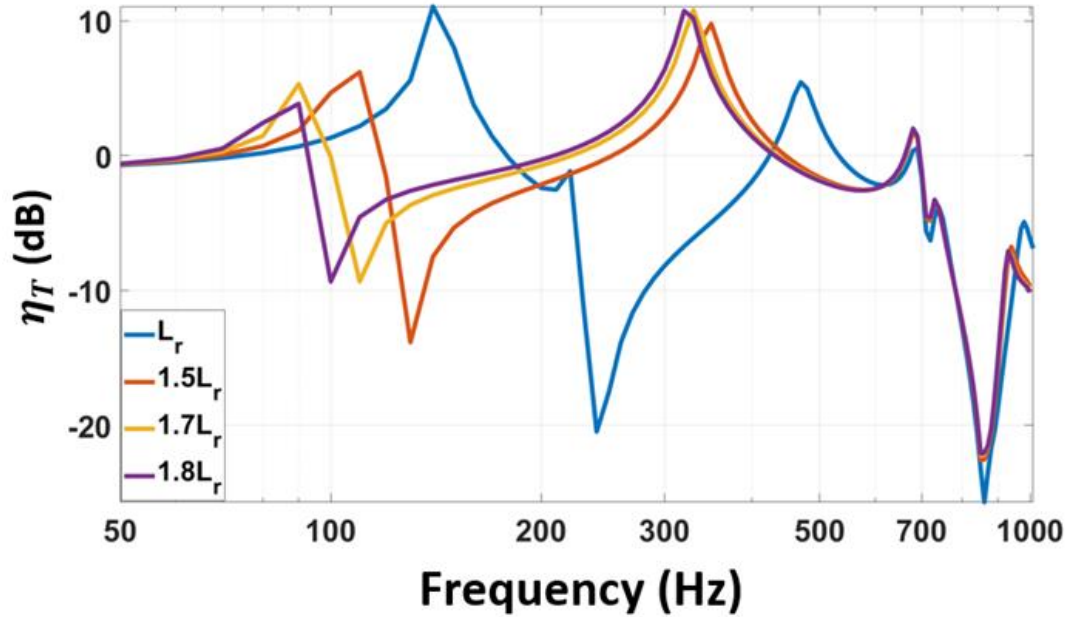
Figure 5-11: The effect of changing the length of the local resonators on vibration transmissibility of the layered metamaterial structure and the position of the first and second bandgaps.

Effects of Variation in the Length of Unit-Cells

Additionally, the impact of a change in the horizontal beams' characteristics on the frequency bandgaps is further investigated. This is done through studying the effect of variations in the length of the unit cell beam, L_u, while the number of resonators is kept the same (i.e., $\alpha = 3$) and their dimensions unaltered (**Figure 5-12**a). Transmissibility results are shown in **Figure 5-12**b. Here, the total length of each of the four horizontal beams, L, is increased from 150mm (when $L_u = 50$mm), to 180mm (when $L_u = 60$mm). A variation in the length of the unit cell's horizontal beam from the original size, $L_u = 50$mm, results in noticeable changes in the second frequency bandgap (**Figure 5-12**b). When the length of the unit cell of the horizontal beams is changed from 60mm to 65mm, as shown in **Figure 5-12**b, the position of the first bandgap experiences slight changes. As shown in **Figure 5-12**b, only the edges of the first bandgap moved slightly from 150

Hz - 380 Hz to 138 HZ - 360 Hz. Moreover, while altering the horizontal beams'

dimensions slightly affects the width of the first frequency bandgap, the depth of its

transmissibility, which is primarily created by the local resonators, remains unchanged.

On the other hand, with a closer look at the second bandgap, one can notice that there are

more prominent changes. Here, the second bandgap becomes broader and shifts to the left

with an increase in the length of the horizontal beams. This is expected because

increasing the length of the unit cell, L_u, makes the total length of the horizontal beam

longer and hence significantly impacts the vibration phase differences between adjacent

unit cells. Thus, altering the horizontal beams' dimensions has a strong impact on the

second bandgap, i.e., the higher frequency bandgap.
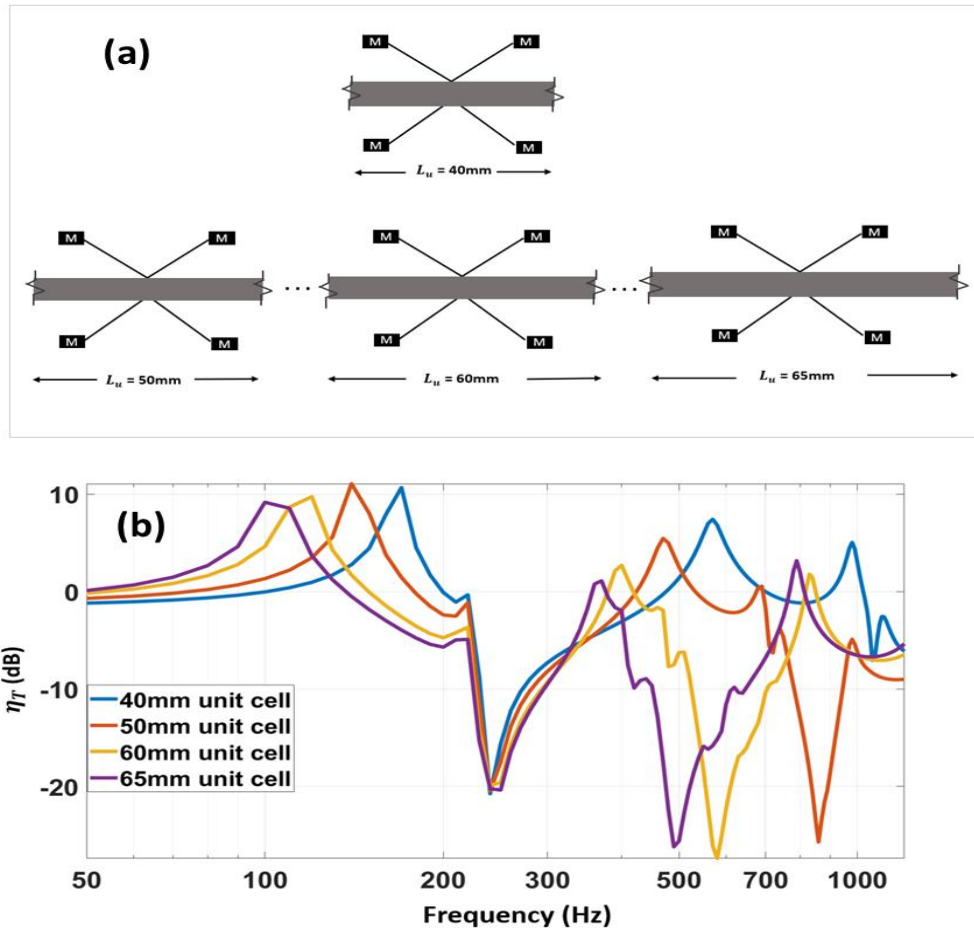
Figure 5-12: Transmissibility graphs showing the effects of changing the length of unit cells on the first and second bandgaps of the layered metamaterial structure: **(a)** Graphical cartoon representation of changes in the length of the unit cell of the layered metamaterial structure. Note: the number of unit cells per horizontal beam remains the same ($\alpha = 3$), but the total length of the horizontal beam is changed as the length of the unit cell is varied, **(b)** the results of a change in length of unit cell, from 40mm to 65mm.

5.4 Comparative Study of Bandgap Development in Single-Beam and Layered-Beam Metamaterial Structures

To further understand the possible advantages offered by layered-beam metamaterial structures over single-beam metamaterial structures, the transmissibility of a single-beam structure shown in **Figure 3-4** is compared with a double-beam

metamaterial structure. For the comparative analysis in this section, for both the single-beam and double-beam structures, the parameters and dimensions in the literature used by both Yu et al. [11] and Zhou et al. [12] and shown in **Table 3-1** are used.

5.4.1   Transmissibility of Single-Beam and Double-Beam Structures

The transmissibility of the single-beam metamaterial structure shown in **Figure 3-4** is analyzed first. Starting with a single horizontal beam metamaterial structure with 8 unit cells (resonators), analyzing **Eq. 3-18** to **Eq. 3-20** numerically and substituting the results into **Eq. 3-19**, yields the FRF transmissibility shown in **Figure 5-13**.
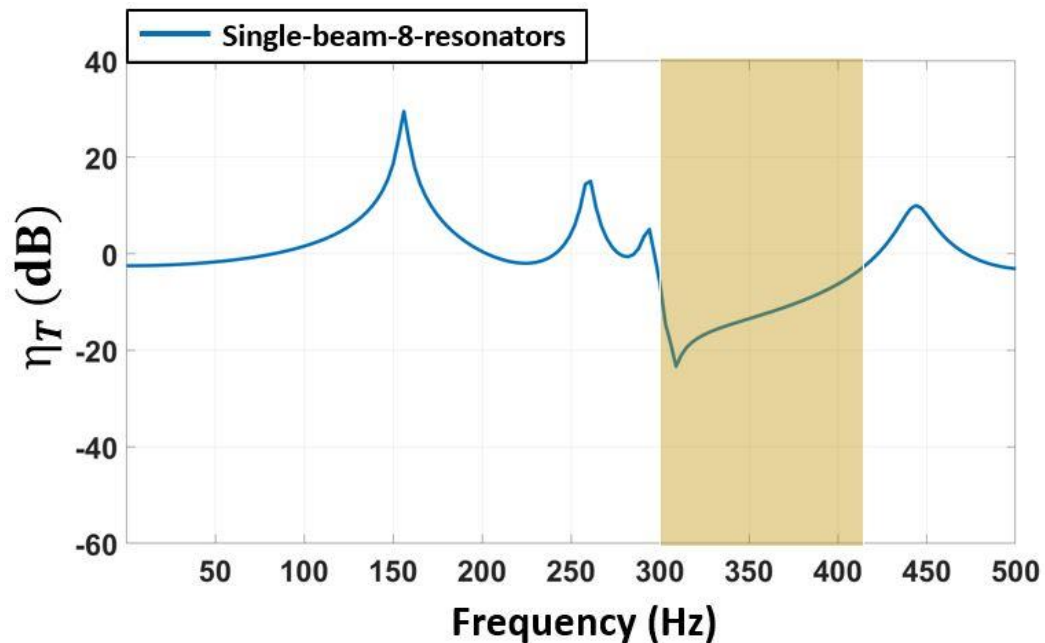
Figure 5-13: Transmissibility Bandgap of a single-horizontal beam metamaterial with 8 unit cells. The material and design parameters were taken from Table 1. Results show a significant frequency bandgap at 300 Hz– 415 Hz.

To generate the transmissibility in **Figure 5-13**, the frequency was swept from 0 Hz to 500 Hz. The input signal from the vibration source was taken from the left end of the horizontal beam ($x = 0$), while the output signal was taken from the right end of the horizontal beam ($x = L$). The results show the presence of one prominent frequency bandgap, i.e. 300 Hz-415 Hz. This bandgap surrounds the resonant frequency of the local resonator, i.e., 309 Hz. The results shown in **Figure 5-13** reveal that the local resonators trap these vibrations within this frequency bandgap; making the bandgap a local-resonator-influenced bandgap. The bandgap in **Figure 5-13** agrees with the frequency bandgap reported and experimentally validated by Yu et al. [11]. Moreover, using the same material dimensions and material properties reported in **Table 3-1**, a similar local resonator bandgap was reported by Zhou et al. [12].

To study the behavior of the bandgap generated by the double-layered metamaterial beam structure **Eq. 3-12**, **Eq. 3-16** and **Eq. 3-2** were applied in developing the transmissibility results. The resulting FRF of the transmissibility, generated using **Eq. 3-17**, is shown in **Figure 5-14**.
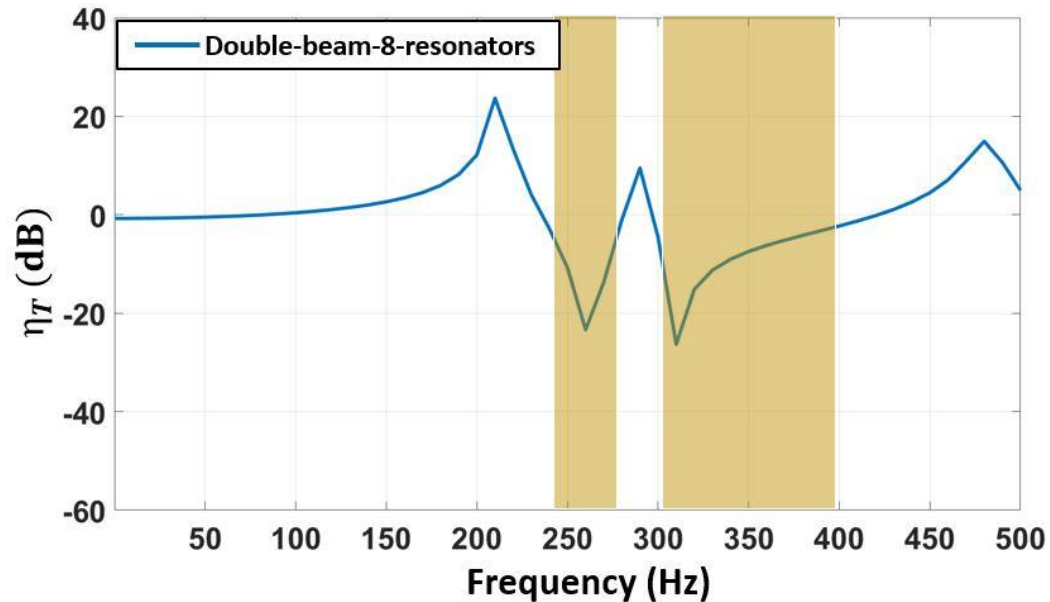
Figure 5-14: Transmissibility and frequency bandgaps generated from model simulations of a double-layered metamaterial beam structure with 8 resonators and using the parameters shown in Table 1. Results show two significant frequency bandgaps, i.e. 238 Hz – 275 Hz and 300 Hz – 410 Hz, marked by the shaded area.

The results from **Figure 5-14** show two major bandgaps at (238 Hz – 275 Hz) and (300 Hz – 410 Hz). These two major bandgaps are marked by the shaded areas in **Figure 5-14**. The first important bandgap occurred at 300 – 410 Hz. This bandgap is maintained within the resonant frequency region of the local resonators, i.e. local-resonator bandgap. In addition to this fundamental frequency bandgap, an extra significant bandgap in the lower frequency region appears in **Figure 5-14**, i.e. 238 Hz – 275 Hz. This second bandgap is the result of the Bragg's scattering phenomena [22] . In effect, with double-layering, the metamaterial beam structure showed the ability to generate multiple bandgaps and at a lower frequency level. Having these multiple bandgaps with some of them happening at lower frequency is desirable for practical applications of metamaterial structures [14].

Comparing the results from **Figure 5-13** and **Figure 5-14**, the advantage offered by a double-beam layered metamaterial beam structure over a single-beam metamaterial structure is evident. First, **Figure 5-14** shows a clear additional lower frequency bandgap in double-layered metamaterial structure, i.e. 238 Hz – 275 Hz. Moreover, **Figure 5-14** exhibits two frequency bandgaps, i.e. 238 Hz – 275 Hz and 300 – 410 Hz, for the double-layered metamaterial structure, compared to a single frequency bandgap, i.e. 300 Hz– 415 Hz in the single-beam metamaterial structure shown in **Figure 5-13**. This is particularly useful in a situation where a specific frequency range is required while an extra bandgap is also desirable. It is worth noting that in Zhou et al. [12] a low frequency bandgap in the single beam metamaterial was achievable using the negative stiffness design adopted in their work. This negative stiffness resulted in only a single frequency bandgap. Thus, a main advantage of the double-beam layered metamaterial structure presented in this article is the ability to create a low frequency bandgap in addition to the local-resonator frequency bandgap as shown in **Figure 5-14**.

5.4.2   <u>Additional Advantages of Layered Metamaterial Structures</u>

To gain more insight on the comparative differences between single-beam and layered-beam metamaterial structures, the effect of increasing the number of local resonators per beam is explored next. Here, the number of local resonators that are attached to the single-beam metamaterial structure, shown in **Figure 3-4**, is increased from 8 to 12 and then 16. In effect, the number of unit-cells increased while the length of unit-cells remains the same. This leads to changes in the overall length of the horizontal beams. The results are shown in **Figure 5-15**.
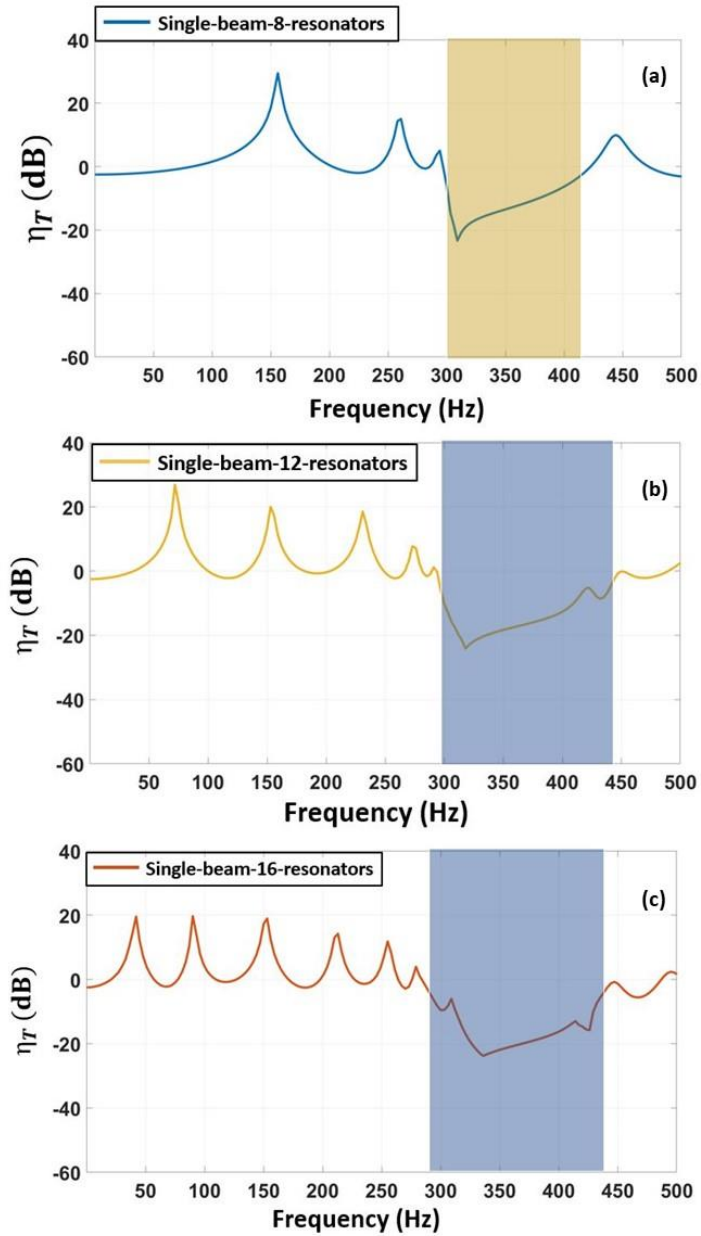
Figure 5-15: Transmissibility and frequency bandgaps of a single-beam metamaterial structure obtained using model simulations when the number of local resonators is increased: (**a**) A single-beam metamaterial structure with 8 local resonators, (**b**) A single-beam metamaterial structure with 12 local resonators, and (**c**) A single-beam metamaterial structure with 16 local resonators.

Figure 5-15 shows that a single notable frequency bandgap is developed when the number of local resonators that are attached to the beam is increased from 8 to 16. The frequency bandgaps, marked by the shaded area in **Figure 5-15**, are 300 Hz– 415 Hz, 298-438 Hz, and 296 - 438 Hz for 8, 12 and 16 local resonators, respectively. No additional significant frequency bandgaps open up when the number of local resonators is increased from 8 to 16 as shown in **Figure 5-15**. These single frequency bandgaps correspond to the region of the resonant frequency of the local resonators. Also, the results from **Figure 5-15** show that the width of the local resonator bandgap becomes broader when the number of local resonators increased from 8 to 12 and then 16 resonators. This broadband frequency bandwidth can be attributed to the merging of small Bragg's scattering bandgaps that are developing close to the local resonator bandgap with the fundamental local resonator bandgap. This widening of central local resonator bandgap as a result of Bragg's scattering bandgaps developing close to it is called coupled-resonance-Bragg's bandgap and has been reported by multiple researchers in literature [22], [23], [42].

In a similar fashion, the effect of increasing the number of local resonators per horizontal beam on the transmissibility of the double-beam metamaterial structure, is analyzed next. **Figure 5-16** displays the frequency bandgaps obtained when the number of local resonators is increased from 8 to 16 per horizontal beam.
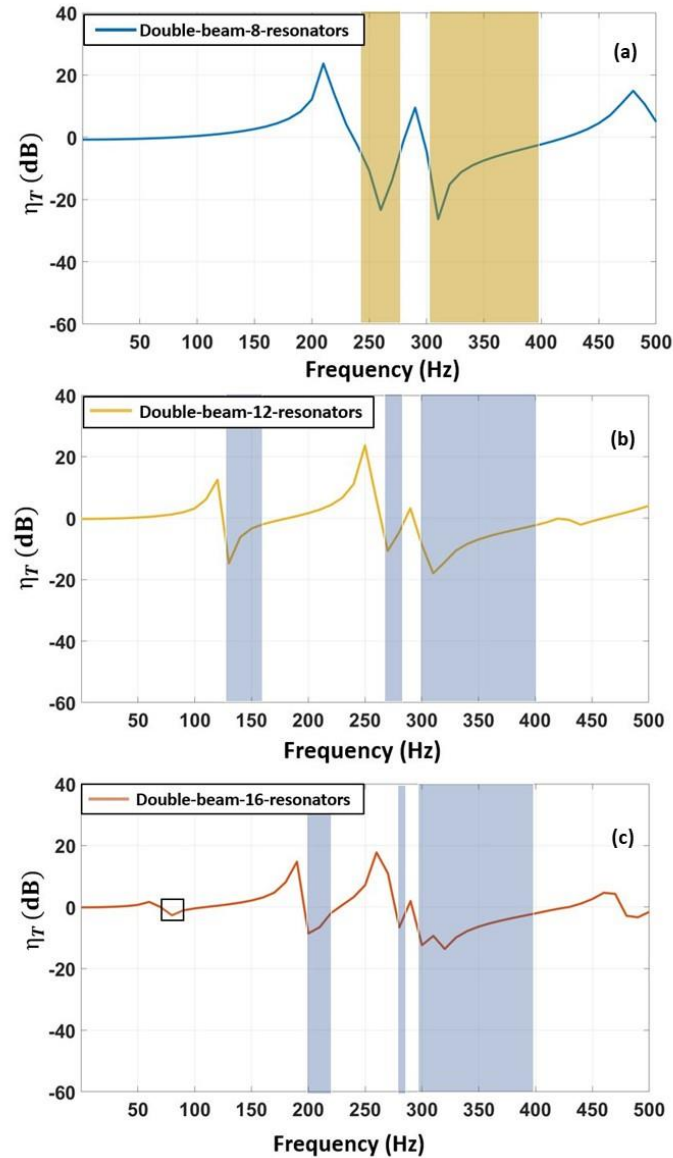
Figure 5-16: Transmissibility of a double-beam metamaterial structure when the number of local resonators per horizontal beam is increased: **(a)** A double-beam metamaterial structure with 8 local resonators, **(b)** A double-beam metamaterial structure with 12 local resonators, and **(c)** A double-beam metamaterial structure with 16 local resonators.

Figure 5-16 shows two main outcomes. First, a major broad frequency bandgap

lives near resonance frequency of the local resonators, i.e. 298 Hz – 410 Hz for 8, 12 and

16 local resonators, respectively. These frequency bandgaps did not witness a significant

change in their width as the number of local resonators increased. This is likely because

there was no alteration to the shape and design of the local resonators. Moreover, as the number of local resonators per horizontal beam is increased from 8 to 16 additional bandgaps opened up. These additional bandgaps tend to exist in the lower frequency region. For example, as shown in **Figure 5-16**, a second frequency bandgap opened up at 238 Hz – 275 Hz, 267 Hz – 281 Hz, and 279 Hz - 286 Hz for 8, 12 and 16 local resonators, respectively. **Figure 5-16**b, a third bandgap opened up at 126 – 157 Hz. This opening of extra bandgap at the lower frequency in layered-beam metamaterial structure as the number of resonators increases has been witnessed in another generic work on layered-metamaterial bandgaps [54]. It is of importance to note that increasing the number of local resonators (unit-cells) per horizontal beam comes with an increase in the overall vertical linking beam. Increased forces act on the beam; increasing the overall internal changes on the structure in layered-metamaterial beam structures. In **Figure 5-16**c, in addition to the three major bandgaps, marked by the shaded area, the sign of a fourth bandgap at frequency below 100 Hz begins to open-up. Though this is not considered a major bandgap because the depth is not significant enough, following a similar approach adopted by Zhou et al, it is enclosed by the square in **Figure 5-16**c. These extra bandgaps are likely the result of Bragg's scattering phenomena. Additionally, as the number of local resonators is increased from 8 to 16, the transmissibility depth of the fundamental local resonator bandgap (292-430 Hz) decreased. This is mainly due to the increase in the number of vertical beams as the number of unit cells increased. That is, the vertical beams make the metamaterial structure stiffer.

The advantage of increasing the number of local resonators that are attached to the double-beam metamaterial structure, shown in **Figure 5-16**, compared to increasing

the number of local resonators that are attached to the single-beam metamaterial

structure, shown in **Figure 5-15**, is evident. As the number of local resonators in the

double-beam metamaterial structure is increased, the number of vertical beams

connecting these beams increases as well. This, consequently, manifests the development

of Bragg's scattering frequency bandgaps in the double-beam metamaterial structure.

This leads to the development of multiple frequency bandgaps in the double-beam

metamaterial structure.
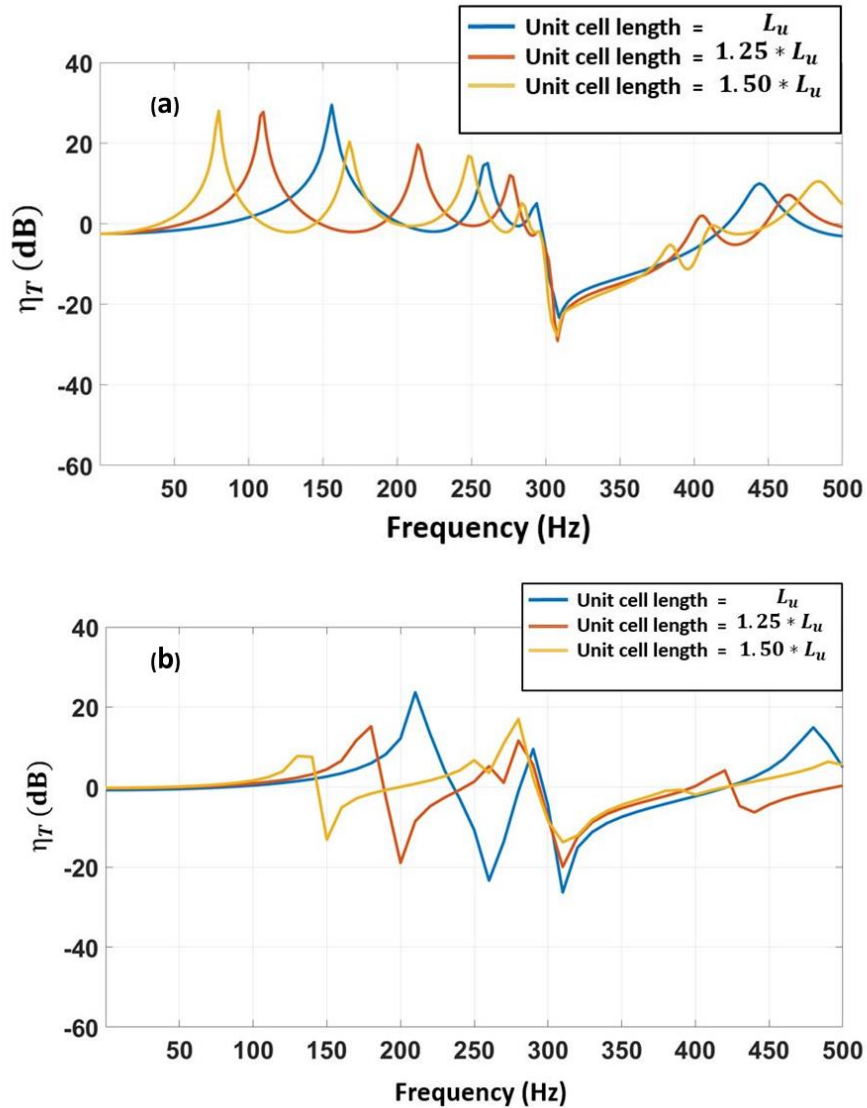
Figure 5-17: The effect of length of unit cells on transmissibility and frequency bandgaps: **(a)** A single-beam metamaterial structure with 8 local resonators per horizontal beam, **(b)** A double-beam metamaterial structure with 8 local resonators per horizontal beam. The lengths of the unit-cell are changed from L_u, to $1.25 \; x \; L_u$ and $1.50 \; x \; L_u$.

Next, the effect of the length of unit cells on the frequency bandgaps is investigated. In **Figure 5-17**, the length of the unit cell L_u is increased by 25% and 50%, respectively. Here, the number of local resonators per horizontal beam remained fixed at 8 and the design of local resonators was unaltered. In **Figure 5-17**a, the results show that

as the unit-cell's length of the single-beam metamaterial structure was varied, no significant extra bandgaps opened up. The region of the local resonator bandgap remained mostly unaltered when the length of the unit cell was changed. However, in **Figure 5-17**b, results show that altering the unit-cell's length for a double-beam metamaterial structure leads to development of noticeable lower frequency bandgaps. For example, increasing the length of the unit cell by 25% resulted in a low frequency bandgap around 190 Hz – 225 Hz in addition to the fundamental local-resonator influenced frequency bandgap at 298 Hz – 410 Hz. In both **Figure 5-17a** and **Figure 5-17**b, the length of the unit-cell L_u was increased while the number of local resonators per horizontal beam remained unaltered. A 25% increase in the length of the unit-cell for double-layered structure shifted the Bragg's scattering lower frequency bandgap from 238 Hz – 275 Hz to 190 – 225Hz Hz. This is not uncommon, as multiple works in literature have shown that an increase in the length of unit-cells while the number of unit-cells remained constant leads to the development of Bragg's bandgap at the lower frequencies below the central local resonator bandgap[22], [23], [42]. Moreover, one can notice that the number of bandgaps generated by altering the length of the unit cell, i.e. **Figure 5-17**b, is less than the number of bandgaps generated from increasing the number of local resonators per beam, i.e. **Figure 5-16**. Nonetheless, as shown in **Figure 5-17**b, changing the length of the unit cell offers a good alternative for lowering frequency bandgaps when it is desired to keep the number of local resonator constant. However, it has been noted in literature that as the number of unit-cells is fixed while the length of unit-cells vary, the damping effect decreases with decrease in frequency [9], [22], [23]. In applications where attempts to lower the transmissibility bandgap by increasing the

number of local resonators is not feasible, small changes to the length of the unit cells can be a viable option. This can be done while maintaining a fixed number of local resonators per horizontal beam. In conclusion, while changing the stiffness and design of the local resonators may offer a route for lowering the frequency bandgaps [11], [12], [23], the work presented in this article offers an additional venue for controlling and adding more frequency bandgaps through layering of metamaterial structures.

CHAPTER 6

CONCLUSIONS

The scope of this doctorate project covered the development of a generic modelling approach to layered-beam metamaterial structures, the validation of the model using predictive dispersion curves developed both through COMSOL and Eigen-Value equation. The semi-analytical model was developed to be generic enough for use by any researcher modeling any number of layered metamaterial structure with varying resonators per horizontal beam. The ability of the layered-metamaterial structure to concurrently harvest electric power was studied and the effects of varying design parameters were analyzed. Ultimately, a lot of vital conclusions on the behavior of layered-beam metamaterial structures were derived from this research project. These conclusions are detailed in this section.

6.1   Model Platform for Layered-Beam Metamaterial Structure

In this doctorate project, design criteria and generalized modelling platform for layered metamaterial structures with local resonators have been established. A fundamental semi-analytical model has been developed using Galerkin method and superposition of modes to describe the dynamic response and transmissibility of the layered metamaterial vibration attenuation structure in response to an external vibration. The transverse vibrations of the layered metamaterial beams were represented with Euler-Bernoulli equation of beams. A prototype of the layered metamaterial structure has been

fabricated and validated experimentally. The prototyped layered metamaterial vibration attenuation structure constituents included four horizontal beams, local resonators forming unit cells, and vertical beams linking the horizontal beams together. Each local resonator consisted of cantilevers with tip masses, while horizontal beams were connected to each other via the vertical beams. Results show good agreement between model simulations and experimental data. Results also reveal the roadmap for successful design of layered metamaterial structures. The effects of various core design parameters in the layered metamaterial structure on the first and second frequency bandgaps have been investigated in this work. Main conclusions from the model design of layered metamaterial structures and their parametric analysis studies include:

- The depth, width and position of the local resonator frequency bandgap is primarily determined by the design of the local resonators.

- An increase in the number of local resonators tends to open up extra frequency bandgaps at lower frequencies with the drawback of reducing the depth in vibration transmissibility.

- Another essential factor in shaping the transmissibility curves of these layered metamaterial structures is the horizontal beams hosting the local resonators. Direct changes to the horizontal beams tend to, mainly, affect the higher frequency bandgaps. An increase in the length of the horizontal beams, while the number and design of the local resonators are fixed, noticeably broadens the second frequency bandgap and shifts it to lower frequencies.

- Since most mechanical vibrations occur at low frequencies, i.e., less than 300 Hz, adjusting the design of local resonators within the layered metamaterial structures is more likely to yield desired lower frequency bandgaps.

6.2   Power Output in Dual-Purpose Metamaterial Structures

The literature is replete with attempts by researchers to develop more accurate and better dual-purpose beam-type metamaterial structures for vibration isolation and energy harvesting. While a lot of these efforts have been focused on the use of piezo-electric actuators to convert trapped vibration energy into electricity, this research has gone on to show that magneto-electric actuators are promising alternatives.

Our research work proved that, as anticipated, electric power can be generated at frequencies around the resonant frequency of local resonators in layered metamaterial structures. Electric power outputs of, approximately, 2.5 µW and 0.6 nW were measured at 223 Hz (first bandgap) and 615 Hz (second bandgap) at optimum load resistance of 15 Ω. These results prove that when external vibrations are incident on the layered-beam metamaterial structure, most of the vibrational energy is localized within the local resonator bandgap. This vibration localization causes the cantilevers to locally resonate and kinetic energy in these resonating cantilevers to be, effectively, converted into useful electric power through the coils at the free-ends of these cantilevers. Results also show that vibration attenuation and energy harvesting characteristics of the metamaterial structure are coupled. Stronger vibration attenuation has led to enhanced vibration energy harvesting capabilities. Frequency sweep measurements at optimum load resistance of 15 Ω reveal that maximum power generated within the first frequency bandgap reaches, approximately, 5.2 µW at 245 Hz.

Compared to state-of-the-art and reported literature, the layered-beam metamaterial structure studied in this work has shown an order of magnitude improvement in electric power generation, at substantially lower optimum load resistance, while maintaining the ability to attenuate undesired vibrations in a frequency bandgap of 205-257 Hz.

6.3   Bandgap Development Comparison between Single-Beam Structures and Layered-Beam Structures

In order to present a knowledge-base for engineers and researchers developing applications requiring beam-type metamaterial structures, the limitations and advantages of both single-beam metamaterial structures and layered-beam metamaterial structures are presented. The single-beam metamaterial structure presented in this article consists of a free-free horizontal beam with equally spaced local resonators attached to the horizontal beam. This single-beam structure is compared with a double-layered metamaterial beam structure is comprised of two layers of horizontal beams linked by vertical beams. Results from this work show differences between the bandgap developed in single-beam metamaterial structures and layered-beam metamaterial structures. These differences are vital points of interest for designers who are considering the choice of single-beam metamaterial structure or layered-beam metamaterial structure for a specific engineering application. The following conclusions were derived from the comparative study carried out in this work:

- For a single-beam metamaterial structure with equally spaced local resonators of the same design, there is a single notable frequency bandgap near the region of the resonant frequency of the local resonators.

- Increasing the number of local resonators that are attached to the horizontal beam of the single-beam metamaterial structure does not yield multiple bandgaps. Nonetheless, increasing the number of local resonators that are attached to the horizontal beam of the single-beam metamaterial structure may slightly increase the width of the local resonator bandgap. This increase in width is likely due to the merging happening between the fundamental local resonator bandgap and adjacent, smaller, Bragg's scattering bandgaps.

- When it is desirable to maintain the design of the local resonators in the metamaterial structure, layering the horizontal beams offers a means for both lowering the frequency bandgap and developing additional bandgaps.

- While increasing the number of local resonators per horizontal beams in the layered metamaterial leads to the birth of additional lower frequency bandgaps, the same effect is not applicable to single-beam metamaterial structures.

- When increasing the number of local resonators is not practicable in application use cases of beam-type metamaterial structures, small changes to the length of the unit cells can be a viable option. Changes to the length of the unit cells while keeping the number of local resonators constant also leads to lower frequency bandgap.

BIBLIOGRAPHY

[1]   Y. Xia, M. Ruzzene, and A. Erturk, "Bistable attachments for wideband nonlinear vibration attenuation in a metamaterial beam," *Nonlinear Dyn.*, vol. 102, no. 3, pp. 1285–1296, 2020.

[2]   Z. Wang, Q. Zhang, K. Zhang, and G. Hu, "Tunable Digital Metamaterial for Broadband Vibration Isolation at Low Frequency," *Adv. Mater.*, vol. 28, no. 44, pp. 9857–9861, Nov. 2016, doi: https://doi.org/10.1002/adma.201604009.

[3]   T. Jiang and Q. He, "Dual-directionally tunable metamaterial for low-frequency vibration isolation," *Appl. Phys. Lett.*, vol. 110, no. 2, p. 21907, Jan. 2017, doi: 10.1063/1.4974034.

[4]   O. Casablanca *et al.*, "Seismic isolation of buildings using composite foundations based on metamaterials," *J. Appl. Phys.*, vol. 123, no. 17, p. 174903, May 2018, doi: 10.1063/1.5018005.

[5]   K. H. Matlack, A. Bauhofer, S. Krödel, A. Palermo, and C. Daraio, "Composite 3D-printed metastructures for low-frequency and broadband vibration absorption," *Proc. Natl. Acad. Sci.*, vol. 113, no. 30, pp. 8386–8390, 2016.

[6]   K. K. Reichl and D. J. Inman, "Lumped mass model of a 1D metastructure for vibration suppression with no additional mass," *J. Sound Vib.*, vol. 403, pp. 75–89, 2017, doi: https://doi.org/10.1016/j.jsv.2017.05.026.

[7]   A. M. Hawkes, A. R. Katko, and S. A. Cummer, "A microwave metamaterial with integrated power harvesting functionality," *Appl. Phys. Lett.*, vol. 103, no. 16, p. 163901, Oct. 2013, doi: 10.1063/1.4824473.

[8]   P. F. Pai, H. Peng, and S. Jiang, "Acoustic metamaterial beams based on multi-frequency vibration absorbers," *Int. J. Mech. Sci.*, vol. 79, pp. 195–205, 2014, doi: https://doi.org/10.1016/j.ijmecsci.2013.12.013.

[9]   M. Nouh, O. Aldraihem, and A. Baz, "Vibration Characteristics of Metamaterial Beams With Periodic Local Resonances," *J. Vib. Acoust.*, vol. 136, no. 6, Oct. 2014, doi: 10.1115/1.4028453.

[10]   D. Yu, Y. Liu, G. Wang, H. Zhao, and J. Qiu, "Flexural vibration band gaps in Timoshenko beams with locally resonant structures," *J. Appl. Phys.*, vol. 100, no. 12, p. 124901, Dec. 2006, doi: 10.1063/1.2400803.

[11]   D. Yu, Y. Liu, H. Zhao, G. Wang, and J. Qiu, "Flexural vibration band gaps in Euler-Bernoulli beams with locally resonant structures with two degrees of freedom," *Phys. Rev. B*, vol. 73, no. 6, p. 64301, Feb. 2006, doi: 10.1103/PhysRevB.73.064301.

[12]   J. Zhou, K. Wang, D. Xu, and H. Ouyang, "Local resonator with high-static-low-dynamic stiffness for lowering band gaps of flexural wave in beams," *J. Appl. Phys.*, vol. 121, no. 4, p. 44902, Jan. 2017, doi: 10.1063/1.4974299.

[13]   G. Hu, L. Tang, A. Banerjee, and R. Das, "Metastructure With Piezoelectric Element for Simultaneous Vibration Suppression and Energy Harvesting," *J. Vib. Acoust.*, vol. 139, no. 1, 2016, doi: 10.1115/1.4034770.

[14]   Y. Li, E. Baker, T. Reissman, C. Sun, and W. K. Liu, "Design of mechanical metamaterials for simultaneous vibration isolation and energy harvesting," *Appl. Phys. Lett.*, vol. 111, no. 25, p. 251903, 2017.

[15]   S. Krödel, N. Thomé, and C. Daraio, "Wide band-gap seismic metastructures," *Extrem. Mech. Lett.*, vol. 4, pp. 111–117, 2015, doi: https://doi.org/10.1016/j.eml.2015.05.004.

[16]   Y. Chen and L. Wang, "Periodic co-continuous acoustic metamaterials with overlapping locally resonant and Bragg band gaps," *Appl. Phys. Lett.*, vol. 105, no. 19, p. 191907, Nov. 2014, doi: 10.1063/1.4902129.

[17]   N. Fang *et al.*, "Ultrasonic metamaterials with negative modulus," *Nat. Mater.*, vol. 5, no. 6, pp. 452–456, 2006, doi: 10.1038/nmat1644.

[18]   M. S. Kushwaha, P. Halevi, L. Dobrzynski, and B. Djafari-Rouhani, "Acoustic band structure of periodic elastic composites," *Phys. Rev. Lett.*, vol. 71, no. 13, pp. 2022–2025, Sep. 1993, doi: 10.1103/PhysRevLett.71.2022.

[19]   Z. Liu *et al.*, "Locally resonant sonic materials.," *Science*, vol. 289, no. 5485, pp. 1734–1736, Sep. 2000, doi: 10.1126/science.289.5485.1734.

[20]   Z. Liu, C. T. Chan, and P. Sheng, "Analytic model of phononic crystals with local resonances," *Phys. Rev. B*, vol. 71, no. 1, p. 14103, Jan. 2005, doi: 10.1103/PhysRevB.71.014103.

[21] C. Sugino, Y. Xia, S. Leadenham, M. Ruzzene, and A. Erturk, "A general theory for bandgap estimation in locally resonant metastructures," *J. Sound Vib.*, vol. 406, pp. 104–123, 2017, doi: https://doi.org/10.1016/j.jsv.2017.06.004.

[22] Y. Xiao, J. Wen, D. Yu, and X. Wen, "Flexural wave propagation in beams with periodically attached vibration absorbers: Band-gap behavior and band formation mechanisms," *J. Sound Vib.*, vol. 332, no. 4, pp. 867–893, 2013, doi: https://doi.org/10.1016/j.jsv.2012.09.035.

[23] M. Y. Wang and X. Wang, "Frequency band structure of locally resonant periodic flexural beams suspended with force–moment resonators," *J. Phys. D. Appl. Phys.*, vol. 46, no. 25, p. 255502, 2013, doi: 10.1088/0022-3727/46/25/255502.

[24] Z. Wang, P. Zhang, and Y. Zhang, "Locally Resonant Band Gaps in Flexural Vibrations of a Timoshenko Beam with Periodically Attached Multioscillators," *Math. Probl. Eng.*, vol. 2013, p. 146975, 2013, doi: 10.1155/2013/146975.

[25] Y. Liu, D. Yu, L. Li, H. Zhao, J. Wen, and X. Wen, "Design guidelines for flexural wave attenuation of slender beams with local resonators," *Phys. Lett. A*, vol. 362, no. 5, pp. 344–347, 2007, doi: https://doi.org/10.1016/j.physleta.2006.10.056.

[26] J. S. Chen, B. Sharma, and C. T. Sun, "Dynamic behaviour of sandwich structure containing spring-mass resonators," *Compos. Struct.*, vol. 93, no. 8, pp. 2120–2125, 2011, doi: https://doi.org/10.1016/j.compstruct.2011.02.007.

[27] Y. Xiao, J. Wen, and X. Wen, "Broadband locally resonant beams containing multiple periodic arrays of attached resonators," *Phys. Lett. A*, vol. 376, no. 16, pp. 1384–1390, 2012, doi: https://doi.org/10.1016/j.physleta.2012.02.059.

[28] G. Hu, A. C. M. Austin, V. Sorokin, and L. Tang, "Metamaterial beam with graded local resonators for broadband vibration suppression," *Mech. Syst. Signal Process.*, vol. 146, p. 106982, 2021.

[29] Z. Oniszczuk, "Free transverse vibrations of elastically connected simply supported double-beam complex system," *J. Sound Vib.*, vol. 232, no. 2, pp. 387–403, 2000, doi: https://doi.org/10.1006/jsvi.1999.2744.

[30] B. Li, Y. Cheng, Z. Zhu, and F. Zhang, "A closed-form solution for a double infinite Euler-Bernoulli beam on a viscoelastic foundation subjected to harmonic line load," *Earthq. Eng. Eng. Vib.*, vol. 18, no. 1, pp. 129–140, 2019, doi: 10.1007/s11803-019-0494-9.

[31]   B. E. Douglas and J. C. S. Yang, "Transverse compressional damping in the vibratory response of elastic-viscoelastic-elastic beams," *AIAA J.*, vol. 16, no. 9, pp. 925–930, Sep. 1978, doi: 10.2514/3.7595.

[32]   H. V Vu, A. M. Ordonez, and B. H. Karnopp, "Vibration of a double-beam system," *J. Sound Vib.*, vol. 229, no. 4, pp. 807–822, 2000, doi: https://doi.org/10.1006/jsvi.1999.2528.

[33]   M. Abu-Hilal, "Dynamic response of a double Euler–Bernoulli beam due to a moving constant load," *J. Sound Vib.*, vol. 297, no. 3, pp. 477–491, 2006, doi: https://doi.org/10.1016/j.jsv.2006.03.050.

[34]   W. Anigbogu and H. Bardaweel, "A Metamaterial-Inspired Structure for Simultaneous Vibration Attenuation and Energy Harvesting," *Shock Vib.*, vol. 2020, p. 4063025, 2020, doi: 10.1155/2020/4063025.

[35]   Z. Chen, B. Guo, Y. Yang, and C. Cheng, "Metamaterials-based enhanced energy harvesting: A review," *Phys. B Condens. Matter*, vol. 438, pp. 1–8, 2014.

[36]   M. Carrara, M. R. Cacan, J. Toussaint, M. J. Leamy, M. Ruzzene, and A. Erturk, "Metamaterial-inspired structures and concepts for elastoacoustic wave energy harvesting," *Smart Mater. Struct.*, vol. 22, no. 6, p. 65004, 2013.

[37]   J.-S. Chen, W.-J. Su, Y. Cheng, W.-C. Li, and C.-Y. Lin, "A metamaterial structure capable of wave attenuation and concurrent energy harvesting," *J. Intell. Mater. Syst. Struct.*, vol. 30, no. 20, pp. 2973–2981, 2019.

[38]   M. Gao, Y. Wang, Y. Wang, and P. Wang, "Experimental investigation of non-linear multi-stable electromagnetic-induction energy harvesting mechanism by magnetic levitation oscillation," *Appl. Energy*, 2018, doi: 10.1016/j.apenergy.2018.03.170.

[39]   T. Sharma and A. Tyagi, "Review of Mechanical Modelling of Fixed-Fixed Beams in RF MEMS Switches," in *2013 Third International Conference on Advanced Computing and Communication Technologies (ACCT)*, 2013, pp. 211–214, doi: 10.1109/ACCT.2013.53.

[40]   W. Waichi, A. Azid, and B. Majlis, "Formulation of stiffness constant and effective mass for a folded beam," *Arch. Mech.*, vol. 62, pp. 405–418, 2010.

[41] G. Dong, X. Zhang, S. Xie, B. Yan, and Y. Luo, "Simulated and experimental studies on a high-static-low-dynamic stiffness isolator using magnetic negative stiffness spring," *Mech. Syst. Signal Process.*, vol. 86, pp. 188–203, 2017, doi: https://doi.org/10.1016/j.ymssp.2016.09.040.

[42] L. Liu and M. I. Hussein, "Wave Motion in Periodic Flexural Beams and Characterization of the Transition Between Bragg Scattering and Local Resonance," *J. Appl. Mech.*, vol. 79, no. 1, Nov. 2011, doi: 10.1115/1.4004592.

[43] K. K. Reichl, O. Avci, and D. J. Inman, "Temperature Dependent Damping in Additively Manufactured Polymer Structures," *J. Appl. Comput. Mech.*, vol. 7, no. Special Issue, pp. 993–1008, 2021, doi: 10.22055/jacm.2021.32839.2086.

[44] A. Pilipović, P. Raos, and M. Šercer, "Experimental analysis of properties of materials for rapid prototyping," *Int. J. Adv. Manuf. Technol.*, vol. 40, pp. 105–115, Jan. 2009, doi: 10.1007/s00170-007-1310-7.

[45] J. Mueller and K. Shea, *The effect of build orientation on the mechanical properties in inkjet 3D-printing*. 2015.

[46] R. Singh, "Process capability study of polyjet printing for plastic components," *J. Mech. Sci. Technol.*, vol. 25, no. 4, pp. 1011–1015, 2011, doi: 10.1007/s12206-011-0203-8.

[47] J. Mueller, S. E. Kim, K. Shea, and C. Daraio, "Tensile Properties of Inkjet 3D Printed Parts: Critical Process Parameters and Their Efficient Analysis." Aug. 02, 2015, doi: 10.1115/DETC2015-48024.

[48] C. Lee, D. Stamp, N. R. Kapania, and J. O. Mur-Miranda, "Harvesting vibration energy using nonlinear oscillations of an electromagnetic inductor," in *Proc.SPIE*, Apr. 2010, vol. 7683, [Online]. Available: https://doi.org/10.1117/12.849895.

[49] D. F. Berdy, D. J. Valentino, and D. Peroulis, "Design and optimization of a magnetically sprung block magnet vibration energy harvester," *Sensors Actuators A Phys.*, vol. 218, pp. 69–79, 2014, doi: https://doi.org/10.1016/j.sna.2014.06.011.

[50] S. Dhote, Z. Yang, K. Behdinan, and J. Zu, "Enhanced broadband multi-mode compliant orthoplanar spring piezoelectric vibration energy harvester using magnetic force," *Int. J. Mech. Sci.*, vol. 135, pp. 63–71, 2018, doi: https://doi.org/10.1016/j.ijmecsci.2017.11.012.

[51]   X. Xu, M. V Barnhart, X. Li, Y. Chen, and G. Huang, "Tailoring vibration suppression bands with hierarchical metamaterials containing local resonators," *J. Sound Vib.*, vol. 442, pp. 237–248, 2019.

[52]   R. Zhu, X. N. Liu, G. K. Hu, C. T. Sun, and G. L. Huang, "A chiral elastic metamaterial beam for broadband vibration suppression," *J. Sound Vib.*, vol. 333, no. 10, pp. 2759–2773, 2014.

[53]   K. H. Sun, J. E. Kim, J. Kim, and K. Song, "Sound energy harvesting using a doubly coiled-up acoustic metamaterial cavity," *Smart Mater. Struct.*, vol. 26, p. 75011, Jul. 2017, doi: 10.1088/1361-665X/aa724e.

[54]   W. Anigbogu, H. Nguyen, and H. Bardaweel, "Layered Metamaterial Beam Structures With Local Resonators for Vibration Attenuation: Model and Experiment," *Front. Mech. Eng.*, vol. 7, p. 93, 2021, doi: 10.3389/fmech.2021.768508.